THE JOURNAL OF BIOLOGICAL CHEMISTRY

Vol. 279, No. 24, Issue of June 11, pp. 25204–25210, 2004
Printed in U.S.A.

A Constitutively Active Arylhydrocarbon Receptor Induces Growth Inhibition of Jurkat T Cells through Changes in the Expression of Genes Related to Apoptosis and Cell Cycle Arrest*

Received for publication, February 26, 2004, and in revised form, March 23, 2004
Published, JBC Papers in Press, April 6, 2004, DOI 10.1074/jbc.M402143200

Tomohiro Ito‡, Shin-ichi Tsukumo‡, Norio Suzuki§, Hozumi Motohashi§, Masayuki Yamamoto§, Yoshiaki Fujii-Kuriyama§, Junsei Mimura§, Tien-Min Lin¶, Richard E. Peterson¶, Chiharu Tohyama‡, and Keiko Nohara‡‖

From the ‡Environmental Health Sciences Division, National Institute for Environmental Studies, Tsukuba 305-8506, Japan, the §Center for Tsukuba Advanced Research Alliance, University of Tsukuba, Tsukuba 305-8575, Japan, and the ¶School of Pharmacy, University of Wisconsin, Madison, Wisconsin 53705

2,3,7,8-Tetrachlorodibenzo-*p*-dioxin (TCDD) is known to suppress T cell-dependent immune reactions through the activation of the arylhydrocarbon receptor (AhR). Our previous findings suggest that TCDD inhibits the activation and subsequent expansion of T cells following antigen stimulation in mice, leading to a decreased level of T cell-derived cytokines involved in antibody production. In the present study, we investigated the effects of activated AhR on T cells by transiently expressing a constitutively active AhR (CA-AhR) mutant in AhR-null Jurkat T cells. In agreement with our previous findings, CA-AhR markedly inhibited the growth of Jurkat T cells. The inhibited cell growth was found to be concomitant with both an increase in the annexin V-positive apoptotic cells and the accumulation of cells in the G_1 phase. The growth inhibition was also shown to be mediated by both xenobiotic response element (XRE)-dependent and -independent mechanisms, because an A78D mutant of the CA-AhR, which lacks the ability of XRE-dependent transcription, partially inhibited the growth of Jurkat T cells. Furthermore, we demonstrated that CA-AhR induces expression changes in genes related to apoptosis and cell cycle arrest. These expression changes were shown to be solely mediated in an XRE-dependent manner, because the A78D mutant of the CA-AhR did not induce them. To summarize, these results suggest that AhR activation causes apoptosis and cell cycle arrest, especially through expression changes in genes related to apoptosis and cell cycle arrest by the XRE-dependent mechanism, leading to the inhibition of T cell growth.

2,3,7,8-Tetrachlorodibenzo-*p*-dioxin (TCDD)[1] is known to exert a variety of toxicities such as reproductive toxicity, immunotoxicity, teratogenicity, and neurotoxicity (1, 2). Previous studies using arylhydrocarbon receptor (AhR) knock-out mice indicate that most, if not all, of the TCDD-induced toxicity is mediated by the AhR, a basic helix-loop-helix periodicity/ARNT/single-minded (PAS) transcription factor (3, 4). In the absence of a ligand, the AhR is located in the cytoplasm in association with heat shock protein 90, X-associated protein 2, and heat shock protein 90 co-chaperone p23 (5). Once a ligand, such as TCDD, binds to the AhR, the complex is translocated into the nucleus where it forms a heterodimer with an AhR nuclear translocator (ARNT). The AhR/ARNT heterodimer binds to specific DNA sequences termed xenobiotic response elements (XREs), and it enhances the expression of genes such as cytochrome P-450 1A1 (*CYP1A1*) (4, 6). On the other hand, it has also been shown that the ligand-activated AhR directly interacts with retinoblastoma protein (RB) (7, 8) and NF-κB (RelA) (9), and their direct interactions modulate the signaling pathways involved in many physiological functions. Although many studies have been conducted, the precise mechanism for individual toxicities of TCDD remains to be clarified.

As regards immunotoxicity, TCDD induces thymus atrophy and suppresses both humoral and cellular immunity in an AhR-dependent manner (10, 11). Recent studies using chimeric mice with the AhR in either hemopoietic or stromal tissues showed that TCDD induces thymus atrophy by directly affecting thymocytes (immature T cells) and not dendritic or stromal cells (12, 13). Additionally, it has been suggested that TCDD-induced thymus atrophy can be attributed to the inhibition of G_1/S cell cycle progression in thymocytes at the double negative stages of T cell development (12). In terms of cellular immunity, it has been reported that full suppression of the cytotoxic T lymphocyte response by TCDD required AhR expression in both $CD4^+$ and $CD8^+$ T cells; this indicates that T cells are direct targets of TCDD (14). With regard to the suppressive effect of TCDD on humoral immunity, primary effects on both B cells and T cells have been reported by several groups (11, 15). Recently, we showed that TCDD considerably reduces the production of the T cell growth factor IL-2 and $CD4^+$ type 2 helper T cell-derived cytokines prior to the inhibition of antibody suppression in mice immunized with ovalbumin (16–18). Furthermore, TCDD suppressed the increase in the number of T cells in the spleen, following immunization. This suggests

* This work was supported by grants from the Core Research for Evolutional Science and Technology, Japan Science and Technology Agency (to C. T., K. N., T. I., and S. T.) and the Ministry of the Environment. The costs of publication of this article were defrayed in part by the payment of page charges. This article must therefore be hereby marked "*advertisement*" in accordance with 18 U.S.C. Section 1734 solely to indicate this fact.

‖ To whom correspondence should be addressed: National Institute for Environmental Studies, Tsukuba 305-8506, Japan. Tel.: 81-29-850-2500; Fax: 81-29-850-2574; E-mail: keikon@nies.go.jp.

[1] The abbreviations used are: TCDD, 2,3,7,8-tetrachlorodibenzo-*p*-dioxin; AhR, arylhydrocarbon receptor; ARNT, arylhydrocarbon receptor nuclear translocator; XRE, xenobiotic response element; CA-AhR, constitutively active arylhydrocarbon receptor; PAS, periodicity/ARNT/single-minded; RB, retinoblastoma protein; IL-2, interleukin-2; GFP, green fluorescent protein; PI, propidium iodide; RT, reverse transcriptase; CYP1A1, cytochrome P-450 1A1; FACS, fluorescence-activate cell sorting; TGF, transforming growth factor; CDA1, cell division autoantigen-1; GADD45A, growth arrest and DNA-damage-inducible, alpha.

that TCDD inhibits the activation of antigen-specific T cells and their subsequent expansion, which probably leads to deteriorated antibody production (16). All these findings strongly suggest that T cells are a vulnerable target of TCDD toxicity, with regard to not only thymus atrophy and inhibition of cellular immunity but also the suppression of humoral immunity. Our recent finding that primary T cells have functional AhR also supports this mechanism (19).

In the present study, to investigate the effects of activated AhR on T cells and their underlying mechanism, we transiently expressed a constitutively active AhR (CA-AhR) mutant in human leukemic Jurkat T cells, because all the T cell lines examined thus far, including Jurkat T cells, do not have functional AhR (20, 21). We used a CA-AhR mutant lacking the minimal PAS B motif, which is constitutively localized in the nucleus and activates AhR-dependent transcription independent of the ligand (22, 23). We also generated an A78D mutant of the CA-AhR, which lacks the ability of XRE-dependent transcription (24), and examined the involvement of XRE-dependent transcription in the effects of CA-AhR on Jurkat T cells.

EXPERIMENTAL PROCEDURES

Plasmid Construction—pEB6CAGFP (an Epstein-Barr virus-based expression vector for green fluorescent protein (GFP) driven by a CAG promoter) (25) and pEB6CAGMCS (containing multicloning sites) were kindly provided by Dr. Yoshihiro Miwa (University of Tsukuba, Tsukuba, Japan). A CA-AhR cDNA[2] was subcloned into a KpnI-HindIII site of pEB6CAGMCS, and pEB6CAG-CA-AhR-GFP, encoding a CA-AhR fused to GFP, was generated by inserting the SalI-AflII fragment of pEGFP-N3 (Clontech Laboratories, Inc., Palo Alto, CA). To examine whether the effects of CA-AhR on Jurkat T cells are mediated by XRE-dependent transcription, the mutation changing the alanine at position 78 to aspartic acid (A78D) (24) in the CA-AhR was introduced by the use of a QuikChange XL site-directed mutagenesis kit (Stratagene, La Jolla, CA) according to the manufacturer's instructions. A primer with the sequence 5′-GTCAGCTACCTGAGGGACAAGAGCTTCTTTGATG-3′ and its complementary equivalent were employed.

Cell Line, Transient Transfection, and Sorting—Jurkat T cells were obtained from the Cell Resource Center for Biomedical Research (Tohoku University, Sendai, Japan) and maintained in RPMI 1640 (Sigma) supplemented with 10% heat-inactivated fetal bovine serum (Invitrogen), 10 mM HEPES (pH 7.1), 1 mM pyruvate, and 50 μM 2-mercaptoethanol at 37 °C in 5% CO_2. Jurkat T cells (2×10^6 cells) were transiently transfected with 6 μg of pEB6CAGFP, pEB6CAG-CA-AhR-GFP, or pEB6CAG-A78D-GFP using DMRIE-C reagent (Invitrogen) according to the manufacturer's instructions. After 2 days, GFP-positive cells from each transfectant were sorted using a FACSVantage SE (BD Biosciences). The efficiency of the sorting was confirmed using a FACSCalibur (BD Biosciences), and 98–99% of the sorted cells were GFP-positive. The sorted cells were cultured at 1×10^5 cells/ml, and then growth rate, apoptosis, and cell cycle distribution were examined as described below. The results obtained in each experiment were confirmed in another independent experiment, and a set of representative results has been shown under "Results."

Detection of Apoptosis—For the detection of apoptotic cells by annexin V binding and propidium iodide (PI) staining, we used an Annexin V-biotin apoptosis detection kit (BioVision, Palo Alto, CA) according to the manufacturer's instructions, with minor modifications. At 0, 2, and 4 days after sorting, the cells were incubated with biotin-labeled annexin V for 5 min at room temperature. After washing, the cells were incubated with streptavidin-labeled allophycocyanin (SA-APC, BD Biosciences) for 15 min at room temperature. After washing, PI was added, and the cells were analyzed using a FACSCalibur.

Furthermore, the induction of apoptosis was confirmed by apoptotic morphological changes. The sorted cells were cultured for 2 days and then stained with 4 μM bisbenzimide (Hoechst 33342, ICN Biomedicals Inc., Aurora, OH) for 15 min. The apoptotic cells were examined by the changes in their nuclear morphology, *i.e.* nuclear fragmentation, under a UV-visible fluorescence microscope. Approximately over 100 cells were counted in four microscopic fields, and the percentage of apoptotic cells was estimated.

Cell Cycle Analysis—At 0, 2, and 4 days after sorting, the cells were stained with PI using a CycleTEST Plus DNA reagent kit (BD Biosciences) according to the manufacturer's instructions, and their DNA content was measured using a FACSCalibur. The percentages of cells in the G_1, S, and G_2/M phases were analyzed using ModFit software (BD Biosciences).

Affymetrix GeneChip Analysis—Affymetrix GeneChip analysis was performed according to the Affymetrix expression analysis technical manual (Affymetrix, Santa Clara, CA), with some modifications. After sorting, total RNA was isolated using an RNeasy Mini Kit (Qiagen, Chatsworth, CA). Double-stranded cDNA was synthesized from 1 μg of total RNA using SuperScript II reverse transcriptase (Invitrogen) and T7 oligo$(dT)_{24}$ primer (Affymetrix). The double-stranded cDNA was purified by the phenol/chloroform extraction method, followed by ethanol precipitation. The *in vitro* transcription reaction was performed using a BioArray high yield RNA transcript-labeling kit (Enzo Diagnostics, Farmingdale, NY). 15 μg of the biotin-labeled cRNA was fragmented and hybridized to a Human Genome U133A array (Affymetrix). The hybridized probe array was washed, stained, and scanned. The data were analyzed using Affymetrix Microarray Suite 5.0 software. A comparison analysis was performed to obtain genes with at least 2-fold changes in Jurkat T cells expressing CA-AhR-GFP as compared with cells expressing GFP alone.

Semiquantitative RT-PCR—To confirm the gene expression changes observed by the Affymetrix GeneChip analysis, semiquantitative RT-PCR was performed on the double strand cDNA prepared for Affymetrix GeneChip analysis. Primers used in the present study were designed using PRIMER3 (frodo.wi.mit.edu/cgi-bin/primer3/primer3_www.cgi) and NCBI UniSTS (www.ncbi.nlm.nih.gov/entrez/query.fcgi?db=unists), based on human sequences published in the NCBI data base. Primer sequences, PCR cycle numbers, and the annealing temperatures of each gene are shown in Table I. Each double-stranded cDNA was amplified in the exponential phase of PCR using TaKaRa *Taq* (TaKaRa Shuzo Co., Ltd., Tokyo, Japan). The amplification was carried out by an initial incubation at 94 °C for 2 min, followed by 19–30 cycles of 94 °C for 30 s, 55 or 60 °C for 30 s, and 72 °C for 30 s, and a final extension at 72 °C for 7 min. The PCR products were separated in a 1.2% Synergel (Diversified Biotech, Boston, MA) containing 0.5 μg/ml ethidium bromide. The net intensity of the bands was quantified using Kodak EDAS 290. The expression level of each gene was normalized to that of glyceraldehyde-3-phosphate dehydrogenase or β-actin.

RESULTS

CA-AhR Inhibits Growth of Jurkat T Cells—To examine the effect of AhR activation on T cells, we used a CA-AhR mutant lacking the minimal PAS B motif (Fig. 1*A*). The CA-AhR mutant has been reported to form a heterodimer with ARNT and induce XRE-dependent gene expression in Chinese hamster ovary cells and MCF-7 cells in the absence of a ligand (22, 23). First, we examined CYP1A1 expression to confirm that CA-AhR induces XRE-dependent gene expression in Jurkat T cells. Jurkat T cells, which expressed ARNT but not AhR (data not shown), were transiently transfected with an expression vector for either CA-AhR-GFP or GFP alone. Two days after the transfection, GFP-positive cells were sorted and RT-PCR for CYP1A1 mRNA was performed. As shown in Fig. 1*B*, CA-AhR-GFP, but not GFP alone, markedly induced CYP1A1 mRNA expression, indicating that the CA-AhR is functional in Jurkat T cells. In addition, the green fluorescence emitted from CA-AhR-GFP was mainly found in the nuclear compartment (data not shown).

To examine the effect of CA-AhR on the growth rate of Jurkat T cells, the sorted cells were cultured for up to 4 days, and the cell numbers were counted at the indicated times. As shown in Fig. 2, the cells expressing GFP alone increased 10-fold, 4 days after sorting. In contrast, the expression of CA-AhR-GFP completely inhibited the increase in cell numbers up to 4 days after sorting, indicating that the activation of AhR greatly inhibits the growth of Jurkat T cells.

CA-AhR Induces Apoptosis in Jurkat T Cells—Because CA-AhR was shown to induce growth inhibition, we examined whether the expression of CA-AhR induces apoptosis in Jurkat T cells. Apoptotic cells were detected with annexin V, which monitors the appearance of phosphatidylserine on the cell sur-

[2] Y. Fujii-Kuriyama and J. Mimura, unpublished data.

TABLE I
List of primers used for semiquantitative RT-PCR

Description	GenBank™ accession number	Primer sequence (5′–3′)	PCR cycle number	Annealing temperature	Product size
				°C	*bp*
AhR	L19872	TTACCTGGGCTTTCAGCAGT	19	60	506
		AACTGGGGTGGAAAGAATCC			(CA-AhR)
β-Actin	X00351	GAGGCCCAGAGCAAGAGAG	19	60	225
		GGCTGGGGTGTTGAAGGT			
Caspase 8	U58143	CTTGGATGCAGGGGCTTTGACC	23	55	550
		GTTCACTTCAGTCAGGATGG			
CDA1	AF254794	TGAGGAGGAAGGAAGTGAAGA	26	60	171
		TAGTGGGTGGGGGATACAGA			
c-Jun	BC002646	GGTATCCTGCCCAGTGTTGT	25	60	382
		CGCACTAGCCTTTGGTAAGC			
c-Myc	V00568	TCGGATTCTCTGCTCTCCTC	24	60	413
		CGCCTCTTGACATTCTCCTC			
Cyclin G2	U47414	TGGACAGGTTCTTGGCTCTT	28	55	367
		AATACAGATGGTTTTGCTTTTGA			
CYP1A1	X02612	CTTGGACCTCTTTGGAGCTG	30	60	212
		CGAAGGAAGAGTGTCGGAAG			
DUSP6	AB013382	CGATGAACGATGCCTATGAC	29	60	262
		TGCCAAGAGAAACTGCTGAA			
Fas	M67454	CTGCCATAAGCCCTGTCCT	27	60	360
		CAAAGCCACCCCAAGTTAGA			
GADD34	U83981	CCTCCTCTGTCCCTTCGTC	26	60	127
		AGTTGGTCTCAGCCACGC			
GADD45A	M60974	CTGGAGGAAGTGCTCAGCAAAG	27	60	399
		TTGATCCATGTAGCGACTTTCC			
GAPDH	M33197	ACCACAGTCCATGCCATCAC	19	60	452
		TCCACCACCCTGTTGCTGTA			
IL-9 receptor	M84747	TTCACCATCACTTTCCACCA	26	60	370
		AACGCTCCTCCTCTACCACA			
$p21^{waf1}$	U03106	GGGAAGGGACACACAAGAAG	25	60	478
		GGGAGCCGAGAGAAAACAG			
TGF-β receptor II	D50683	CGGCTCCCTAAACACTACCA	27	60	478
		GGTCCCTTCCTTCTCTGCTT			

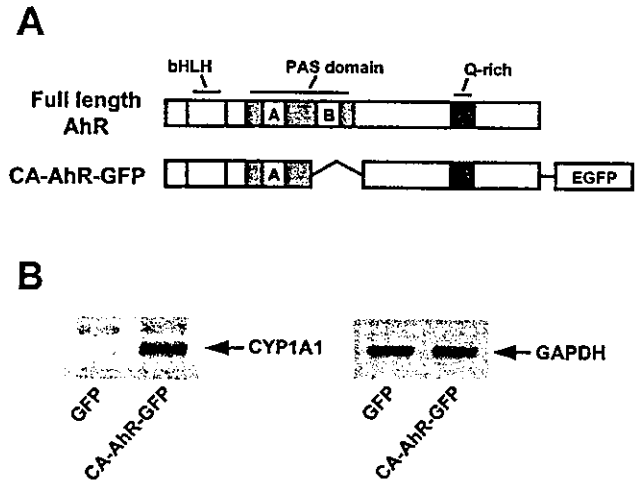

FIG. 1. **Structure of a constitutively active mutant of an arylhydrocarbon receptor (CA-AhR) and CYP1A1 induction in Jurkat T cells expressing CA-AhR.** *A*, the structures of wild-type AhR and a CA-AhR fused to GFP (CA-AhR-GFP) are shown. The CA-AhR lacks the minimal PAS B motif. *B*, the expression vector for either CA-AhR-GFP or GFP alone was transiently transfected into Jurkat T cells using DMRIE-C reagent. Two days after transfection, GFP-positive cells were sorted using a FACSVantage SE. Total RNA was isolated from the cells, and mRNA expression levels of CYP1A1 and glyceraldehyde-3-phosphate dehydrogenase were examined by semiquantitative RT-PCR.

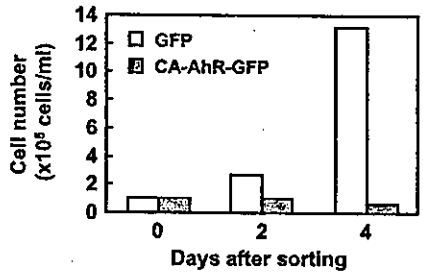

FIG. 2. **CA-AhR inhibits growth of Jurkat T cells.** The expression vector for either CA-AhR-GFP or GFP alone was transiently transfected into Jurkat T cells using DMRIE-C reagent. After 2 days, GFP-positive cells from each transfected cells were sorted using a FACSVantage SE and then cultured at 1×10^5 cells/ml. The cell numbers at the indicated times were determined by trypan blue exclusion.

face during apoptosis. In addition, PI was used to distinguish between early and late apoptosis, because PI is excluded only by live and early apoptotic cells. As shown in Fig. 3, where annexin V-positive, PI-negative cells (*upper left quadrant*) represent early apoptotic cells and annexin V, PI-double positive cells (*upper right quadrant*) represent late apoptotic/necrotic cells, GFP-alone-transfected cells did not show remarkable changes in the ratio of dead cells. On the other hand, CA-AhR-GFP increased the percentage of apoptotic cells, especially 2 and 4 days after sorting. Two days after sorting, the percentage of early apoptotic cells was 3-fold higher in cells expressing CA-AhR-GFP than in those expressing GFP alone. Moreover, 4 days after sorting, CA-AhR-GFP augmented the percentages of early apoptotic cells and late apoptotic/necrotic cells by approximately 8- and 6-fold, respectively, as compared with GFP alone.

Furthermore, the induction of apoptosis was confirmed by nuclear morphological changes. Each group of sorted cells was cultured for 2 days and stained with Hoechst 33342 dye. Fragmented nuclei were observed in a number of cells expressing CA-AhR-GFP (Fig. 4*A*, *arrowheads*), and apoptotic cells reached about 30%; however, the apoptotic cells only reached 10% in cells expressing GFP alone (Fig. 4*B*).

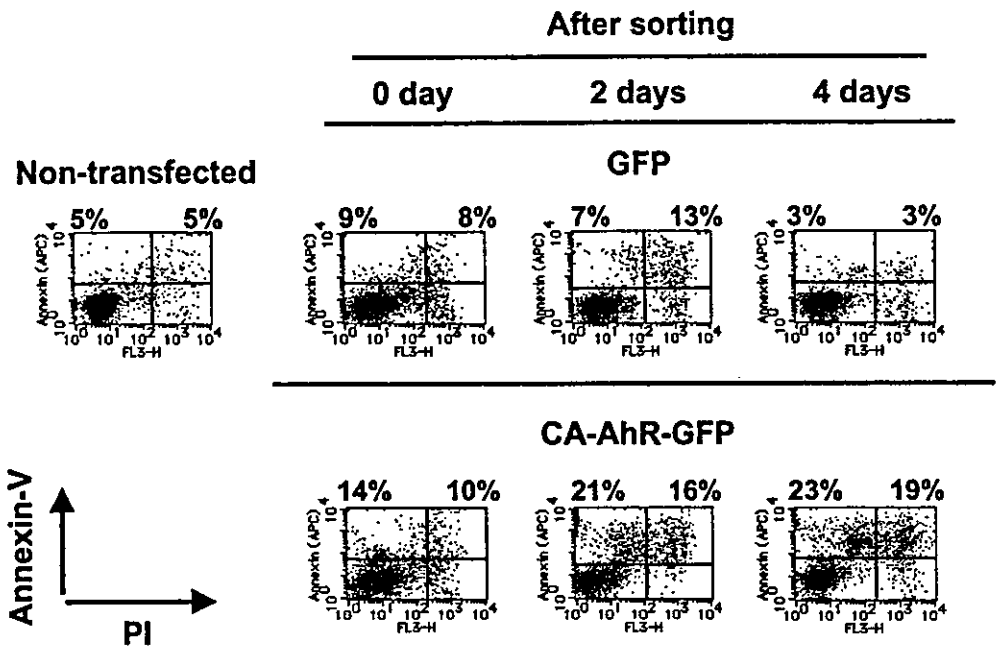

FIG. 3. **CA-AhR induces apoptosis in Jurkat T cells.** The expression vector for either CA-AhR-GFP or GFP alone was transiently transfected into Jurkat T cells using DMRIE-C reagent. After 2 days, GFP-positive cells were sorted from the transfected cells using a FACSVantage SE and then cultured for the indicated time periods. The cells were incubated with biotin-labeled annexin V, followed by staining with SA-APC and PI, and analyzed using a FACSCalibur. The *upper left quadrant* (annexin V-positive, PI-negative) represents early apoptotic cells, whereas the *upper right quadrant* (annexin V, PI-double positive) represents late apoptotic/necrotic cells.

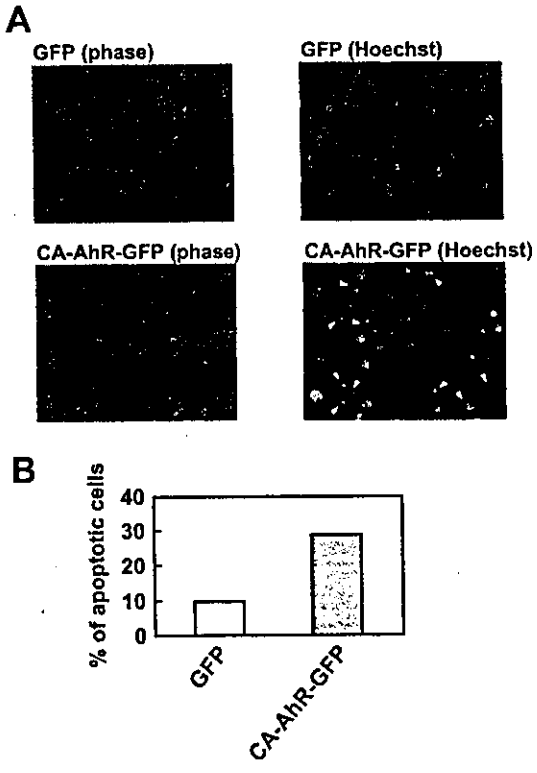

FIG. 4. **CA-AhR induces apoptotic morphological changes in Jurkat T cells.** *A*, the expression vector for either CA-AhR-GFP or GFP alone was transiently transfected into Jurkat T cells using DMRIE-C reagent. After 2 days, GFP-positive cells were sorted from the transfected cells using a FACSVantage SE. The sorted cells were cultured for 2 days and then stained with 4 μM Hoechst 33342 for 15 min. The apoptotic cells were examined by the changes in their nuclear morphology, *i.e.* with fragmentation under a phase-contrast and a UV-visible fluorescence microscope. The *arrowheads* indicate the fragmented nuclei of the apoptotic cells. *B*, approximately over 100 cells were counted in four microscopic fields under a UV-visible fluorescence microscope, and the percentage of the apoptotic cells was estimated.

CA-AhR Induces the Accumulation of Cells in the G_1 Phase—We also investigated the possibility that CA-AhR induces cell cycle arrest. As shown in Fig. 5, in non-transfected Jurkat T cells, 48% of the cells were in the G_1 phase, 37% were in the S phase, and 15% were in the G_2/M phase. Immediately after sorting (0 day), no difference was observed in the DNA profile among non-transfected cells, cells expressing GFP alone, and those expressing CA-AhR-GFP. Two days after sorting, the percentage of cells expressing CA-AhR-GFP rose to 61% in the G_1 phase and correspondingly decreased to 24% in the S phase, whereas no change in cell cycle distribution was observed in cells expressing GFP alone. Four days after sorting, the percentages in the individual phases were not significantly changed from those obtained 2 days after sorting. These results suggest that CA-AhR affects cell cycle progression, especially in the G_1 phase.

The Inhibition of Growth by CA-AhR Is Mediated by Both XRE-dependent and -independent Mechanisms—To elucidate whether the inhibitory effect of CA-AhR on the growth of Jurkat T cells is mediated by an XRE-dependent or -independent mechanism, we generated an A78D mutant of the CA-AhR. The A78D mutant of wild-type AhR is translocated into the nucleus in the presence of TCDD and forms a heterodimer with ARNT. However, it lacks the potential for XRE-driven gene expression due to impaired XRE binding (24). To confirm that the disruption of transcription by A78D mutation is available for the CA-AhR, we examined the effects of A78D mutation introduced into the CA-AhR on localization and gene expression. When either CA-AhR-GFP or A78D mutant of CA-AhR-GFP (A78D-GFP) was transiently expressed in Jurkat T cells, a FACS analysis showed the same GFP expression patterns between both types of transfected cells, before and after sorting (Fig. 6*A*). Furthermore, the mRNA expression of CA-AhR-GFP or A78D-GFP was detected at the same level in both transfected cells by semiquantitative RT-PCR (Fig. 6*B*). The green fluorescence emitted by the GFP was mainly observed in the nuclear compartment in cells expressing A78D-GFP as well as CA-AhR-GFP (data not shown). However, as shown in Fig. 6*B*, only

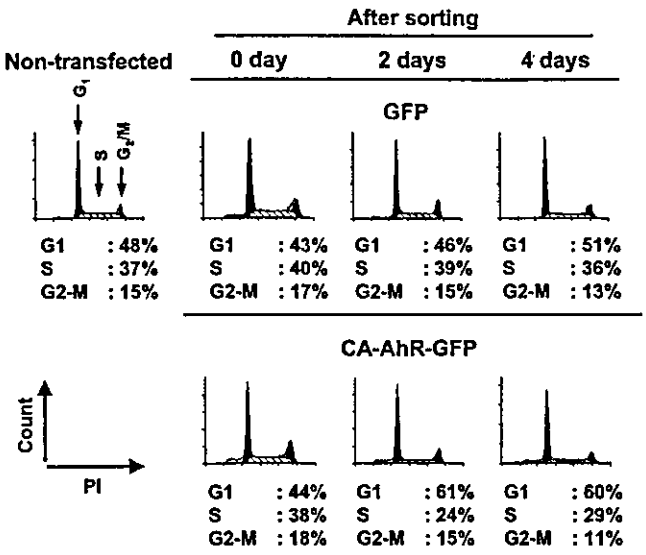

FIG. 5. **CA-AhR increases the percentage of cells in the G_1 phase.** The expression vector for either CA-AhR-GFP or GFP alone was transiently transfected into Jurkat T cells using DMRIE-C reagent. After 2 days, GFP-positive cells were sorted from the transfected cells using a FACSVantage SE and then cultured for the indicated time periods. The cells were stained with PI using a CycleTEST Plus DNA reagent kit, and DNA content was measured using a FACSCalibur. The percentages of cells in the G_1, S, and G_2/M phases were analyzed using ModFit software.

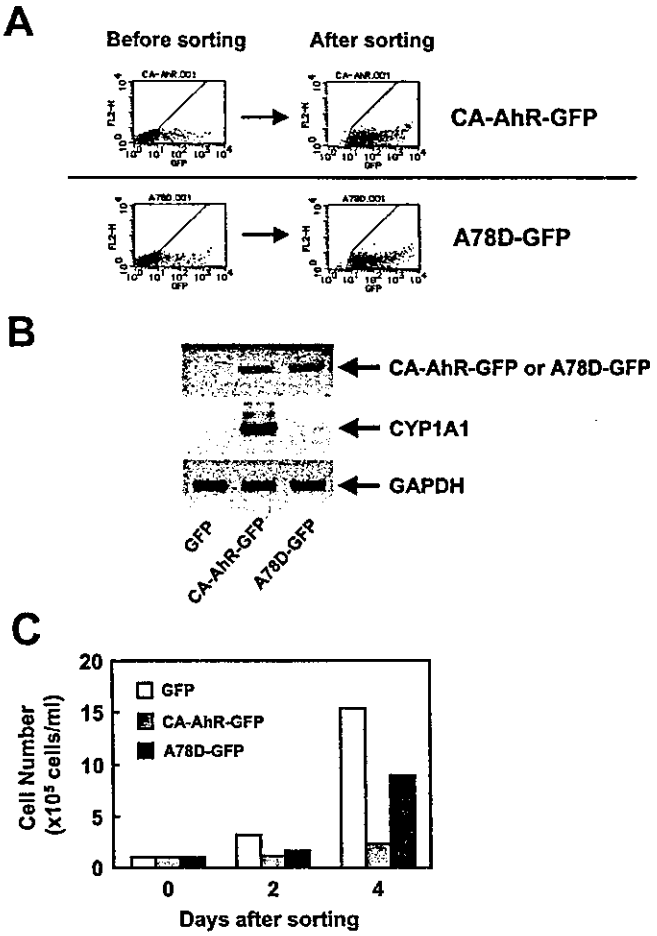

FIG. 6. **CA-AhR inhibits the growth of Jurkat T cells by the XRE-dependent and -independent mechanisms.** *A*, the expression vector for either CA-AhR-GFP, A78D-GFP, or GFP alone was transiently transfected into Jurkat T cells using DMRIE-C reagent. Two days after the transfection, GFP-positive cells were sorted using a FACSVantage SE. The GFP expression of the cells was analyzed before and after sorting, using a FACSCalibur. *B*, total RNA was isolated from the cells and mRNA expression levels of CYP1A1, CA-AhR-GFP, and glyceraldehyde-3-phosphate dehydrogenase were examined by semiquantitative RT-PCR. *C*, the sorted cells were cultured at 1×10^5 cells/ml, and the cell numbers at the indicated times were determined by trypan blue exclusion.

CA-AhR-GFP, but not A78D-GFP, induced CYP1A1 mRNA expression. These observations show that A78D-GFP is constitutively localized in the nucleus in the absence of TCDD, but it cannot induce gene expression by binding to the XRE.

Using these AhR mutants, the XRE dependence of the inhibitory effect of activated AhR was examined. As shown in Fig. 6*C*, CA-AhR markedly inhibited the increase in cell number (in agreement with the data shown in Fig. 2). On the other hand, the A78D mutant only partially inhibited the increase. This result indicates that both XRE-dependent and -independent mechanisms are involved in the CA-AhR-induced growth inhibition.

CA-AhR Induces Expression Changes of Genes Related to Apoptosis and Cell Cycle Arrest by an XRE-dependent Mechanism—Because CA-AhR induced apoptosis and the accumulation in the G_1 phase in Jurkat T cells, we examined whether CA-AhR changes the expression of genes related to apoptosis and cell cycle arrest and whether the regulations of these genes are mediated by XRE-dependent transcription. Two days after transfection, total RNA was isolated from the GFP-positive cells, and the gene expression was analyzed using an Affymetrix GeneChip. Genes related to apoptosis and cell cycle arrest were selected from the genes that showed at least a 2-fold change in gene expression in the cells expressing CA-AhR-GFP, as compared with cells expressing GFP alone, and their expression changes were confirmed by semiquantitative RT-PCR. Furthermore, we determined the relative -fold induction of each of the confirmed genes in cells expressing CA-AhR-GFP and in cells expressing A78D-GFP by a comparison with the cells expressing GFP alone (Fig. 7 and Table II). We found that CA-AhR up-regulates genes related to apoptosis (caspase 8, c-Jun, and Fas) (26, 27) and cell cycle arrest (cyclin G2, growth arrest and DNA-damage-inducible, alpha (GADD45A), $p21^{waf1}$, cell division autoantigen-1 (CDA1), and IL-9 receptor) (28–32). CA-AhR also up-regulated the genes involved in both apoptosis and cell cycle arrest (dual specificity phosphatase 6, GADD34, and TGF-β receptor II) (33–36). On the other hand, c-Myc, which plays an important role in the G_1/S transition (37), was down-regulated in cells expressing CA-AhR-GFP. Furthermore, our results clarified that all the changes in these genes were dependent on transcription through the XRE, because only CA-AhR, but not A78D, induced expression changes of these genes (Fig. 7 and Table II).

DISCUSSION

In the present study, $CD4^+$ T cell line Jurkat T cells were transiently expressed with a CA-AhR, a model of ligand-activated AhR. We demonstrated that CA-AhR remarkably inhibits the growth of Jurkat T cells. We also clarified that CA-AhR induces both apoptosis and accumulation in the G_1 phase, which strongly suggests that these effects induce growth inhibition in Jurkat T cells. Furthermore, we showed that CA-AhR-induced growth inhibition is mediated by both XRE-dependent and -independent mechanisms, using an A78D mutant of the CA-AhR. With regard to the XRE-dependent mechanism, our results demonstrate that CA-AhR induces expression changes in genes related to apoptosis and cell cycle arrest. On the other hand, the XRE-independent growth inhibition, which is caused by the A78D mutant of the CA-AhR, may result from the interaction between CA-AhR and its target molecules. For in-

stance, it has been reported that RB specifically interacts with both an LXCXE motif in PAS B of the AhR and the C-terminal region of the AhR and that their direct interaction inhibits E2F-driven gene expression, leading to G_1 arrest (7, 8, 38). Although the CA-AhR protein lacks a PAS B region containing an LXCXE motif, it possesses the ability to specifically interact with RB through the C-terminal region. The semiquantitative RT-PCR data in our present and previous study (19) suggest that the CA-AhR was expressed in Jurkat T cells at a much higher level than the native AhR in mouse thymocytes and splenocytes. Therefore, we also cannot rule out the possibility that the XRE-independent growth inhibition was due to artifactual effects, such as stress response, of overexpression of the AhR protein in the nucleus. Further studies will be needed to elucidate the mechanism of XRE-independent growth inhibition.

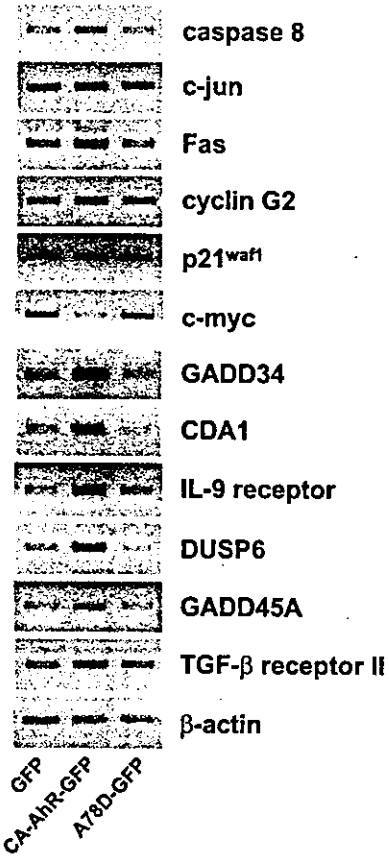

FIG. 7. **CA-AhR induces expression changes of genes related to apoptosis and cell cycle arrest by an XRE-dependent mechanism.** The expression vector for either CA-AhR-GFP, A78D-GFP, or GFP alone was transiently transfected into Jurkat T cells using DMRIE-C reagent. Two days after the transfection, GFP-positive cells were sorted using a FACSVantage SE. Total RNA was isolated from the cells, and gene expression was analyzed using an Affymetrix GeneChip. Genes related to apoptosis and cell cycle arrest were collected from the genes that showed at least a 2-fold change in gene expression in the cells expressing CA-AhR-GFP, as compared with the cells expressing GFP alone, and the expression changes of these genes were confirmed by semiquantitative RT-PCR.

The gene expression analysis suggests the involvement of several signaling pathways in the growth suppression of Jurkat T cells. The increase in Fas and caspase 8 transcripts by CA-AhR suggests that the Fas signaling pathway is involved in the CA-AhR-induced apoptosis. In agreement with our present data, previous studies using mice having a deficiency in the Fas signaling pathway have shown that TCDD decreases the cell number of anti-CD3-activated T cells through a Fas signaling pathway (39, 40). The study by Zeytun *et al.* (40) reported that Fas ligand was up-regulated in the spleen cells of mice exposed to TCDD. However, CA-AhR did not increase the expression level of Fas ligand in Jurkat T cells. This discrepancy between our study and that of Zeytun *et al.* suggests that TCDD-induced up-regulation of Fas ligand is due to the effect on non-T cells in spleen cells. As another apoptosis-related gene, we found that CA-AhR increases TGF-β receptor II transcript. The TGF-β signaling pathway has been reported to induce apoptosis and cell cycle arrest in T cells (36). Although CA-AhR induces no changes in the expression level of the TGF-β family (TGF-β1, β2, and β3) in Jurkat T cells (data not shown), the up-regulation of TGF-β receptor II by AhR activation in T cells may cause an increase in their susceptibility to TGF-β. CA-AhR also regulated a number of genes related to cell cycle arrest. We found that CA-AhR induces expression changes of genes involved not only in G_1 arrest (cyclin G2 and c-Myc) (28, 37) but also in G_2 arrest (GADD45A) (29), in both G_1 and G_2 arrest ($p21^{waf1}$) (30), and in multiphase cell cycle arrest (CDA1) (31). Through a cell cycle analysis, we showed that CA-AhR induced the accumulation in the G_1 phase by culturing for 2 days after sorting. However, further accumulation in the G_1 phase was not found by culturing for 4 days after sorting. These results may suggest

TABLE II

Relative-fold induction of CA-AhR-regulated genes in the XRE-dependent and -independent fashion

Gene expression changes by CA-AhR were examined by Affymetrix GeneChip analysis, and genes related to apoptosis and cell cycle arrest with at least two-fold changes in CA-AhR-GFP-transfected cells, as compared with GFP-alone transfected cells, were selected. Relative expression levels of the selected genes in cells expressing either CA-AhR-GFP or A78D-GFP were determined by semiquantitative RT-PCR.

Description	Change[a]	Functions	CA-AhR, change[b]	A78D, change[c]
			-fold	
Caspase 8	Up	Apoptosis	1.72	0.76
c-Jun	Up	Apoptosis	1.42	0.85
Fas	Up	Apoptosis	2.66	0.62
Cyclin G2	Up	G_1 arrest	2.20	0.78
c-Myc	Down	G_1/S transition	0.29	0.75
GADD45A	Up	G_2 arrest	1.30	0.71
$p21^{waf1}$	Up	G_1 arrest and G_2 arrest	1.98	1.19
CDA1	Up	Growth arrest	2.36	0.73
IL-9 receptor	Up	Growth arrest	4.79	1.33
DUSP6	Up	Apoptosis and growth arrest	3.00	0.57
GADD34	Up	Apoptosis and growth arrest	2.18	0.69
TGF-β receptor II	Up	Apoptosis and growth arrest	1.79	0.89

[a] Gene expression changes were determined by Affymetrix GeneChip analysis.

[b] Relative gene expression level was determined in cells expressing CA-AhR-GFP, as compared with cells expressing GFP alone, by semiquantitative RT-PCR.

[c] Relative gene expression level was determined in cells expressing A78D-GFP, as compared with cells expressing GFP alone, by semiquantitative RT-PCR.

that CA-AhR causes alteration of the G_1/S transition at an early stage and then inhibits cell cycle progression at various stages of the cell cycle.

With regard to how CA-AhR regulates the transcription of these genes, a search for the human genome sequences of the NCBI demonstrated that the 5′-flanking regions of GADD34, IL-9 receptor, CDA1, and c-Jun genes contain the core consensus sequence of XRE (5′-TNGCGTG-3′ or 5′-CACGCNA-3′), suggesting that these genes are directly regulated by activated AhR through the XRE, whereas other genes seem to be regulated by indirect mechanisms. The expression of Fas, GADD45A, $p21^{waf1}$, and caspase 8 are known to be up-regulated by the activation of p53 (41, 42). Recently, it has been reported that GADD34 induces phosphorylation of p53 and enhances $p21^{waf1}$ expression (35). Likewise, CA-AhR may up-regulate genes such as Fas, GADD45A, and caspase 8 through induction of GADD34 and following p53 activation. In addition, it has been reported that the induction of CYP1A1 causes DNA damage (43), probably leading to the activation of p53. Therefore, this p53-dependent pathway may be involved in CA-AhR-induced apoptosis and cell cycle arrest.

Previous studies have reported that TCDD induces apoptosis in AhR-null T cell clones, including Jurkat T cells, in an AhR-independent manner (20, 44). However, Jurkat T cells used in this study were not susceptible to apoptosis even in the presence of 10 nM TCDD (data not shown). Although the reason for the discrepancy is unclear, our results well indicate that activated AhR is essential for the inhibition of T cell growth by TCDD, in agreement with the findings that AhR expression is indispensable for TCDD-induced immunosuppression *in vivo* (10, 11).

In summary, we demonstrated that CA-AhR induces the growth inhibition of Jurkat T cells, with an increase in apoptosis and the accumulation of the cells in the G_1 phase. Furthermore, we showed that both XRE-dependent and -independent mechanisms are involved in CA-AhR-induced growth inhibition and that CA-AhR regulates the expression of several genes related to apoptosis and cell cycle arrest in an XRE-dependent manner. Further studies will aim to identify target gene(s) and protein(s) mainly responsible for the inhibition of T cell growth by the XRE-dependent and -independent mechanisms. $CD4^+$ helper T cells play an important role in both humoral and cellular immunity, where TCDD inhibited the increase in the number of $CD4^+$ T cells, following immunization (16, 45). The present data may provide a mechanism for the suppression of both humoral and cellular immunity.

Acknowledgments—We gratefully acknowledge Drs. Yoshihiro Miwa and Junko Tanaka (University of Tsukuba) for providing pEB6 expression vectors and technical advice on plasmid construction, and Kazuhiro Shiizaki (National Institute for Environmental Studies) for technical advice on point mutation in the AhR. We also thank Michiyo Matsumoto for their excellent technical and Kyoko Nakazawa for secretarial assistance.

REFERENCES

1. Birnbaum, L. S., and Tuomisto, J. (2000) *Food Addit. Contam.* **17,** 275–288
2. Tohyama, C. (2002) *Environ. Sci.* **9,** 37–50
3. Fernandez-Salguero, P. M., Hilbert, D. M., Rudikoff, S., Ward, J. M., and Gonzalez, F. J. (1996) *Toxicol. Appl. Pharmacol.* **140,** 173–179
4. Mimura, J., and Fujii-Kuriyama, Y. (2003) *Biochim. Biophys. Acta* **1619,** 263–268
5. Petrulis, J. R., and Perdew, G. H. (2002) *Chem. Biol. Interact.* **141,** 25–40
6. Whitlock, J. P., Jr. (1999) *Annu. Rev. Pharmacol. Toxicol.* **39,** 103–125
7. Puga, A., Barnes, S. J., Dalton, T. P., Chang, C. Y., Knudsen, E. S., and Maier, M. A. (2000) *J. Biol. Chem.* **275,** 2943–2950
8. Ge, N.-L., and Elferink, C. J. (1998) *J. Biol. Chem.* **273,** 22708–22713
9. Tian, Y., Ke, S., Denison, M. S., Rabson, A. B., and Gallo, M. A. (1999) *J. Biol. Chem.* **274,** 510–515
10. Vorderstrasse, B. A., Steppan, L. B., Silverstone, A. E., and Kerkvliet, N. I. (2001) *Toxicol. Appl. Pharmacol.* **171,** 157–164
11. Kerkvliet, N. I. (2002) *Int. Immunopharmacol.* **2,** 277–291
12. Laiosa, M. D., Wyman, A., Murante, F. G., Fiore, N. C., Staples, J. E., Gasiewicz, T. A., and Silverstone, A. E. (2003) *J. Immunol.* **171,** 4582–4591
13. Staples, J. E., Murante, F. G., Fiore, N. C., Gasiewicz, T. A., and Silverstone, A. E. (1998) *J. Immunol.* **160,** 3844–3854
14. Kerkvliet, N. I., Shepherd, D. M., and Baecher-Steppan, L. (2002) *Toxicol. Appl. Pharmacol.* **185,** 146–152
15. Holsapple, M. P., Snyder, N. K., Wood, S. C., and Morris, D. L. (1991) *Toxicology* **69,** 219–255
16. Ito, T., Inouye, K., Fujimaki, H., Tohyama, C., and Nohara, K. (2002) *Toxicol. Sci.* **70,** 46–54
17. Nohara, K., Fujimaki, H., Tsukumo, S., Inouye, K., Sone, H., and Tohyama, C. (2002) *Toxicology* **172,** 49–58
18. Fujimaki, H., Nohara, K., Kobayashi, T., Suzuki, K., Eguchi-Kasai, K., Tsukumo, S., Kijima, M., and Tohyama, C. (2002) *Toxicol. Sci.* **66,** 117–124
19. Doi, H., Baba, T., Tohyama, T., and Nohara, K. (2003) *Chemosphere* **52,** 655–662
20. Hossain, A., Tsuchiya, S., Minegishi, M., Osada, M., Ikawa, S., Tezuka, F., Kaji, M., Konno, T., Watanabe, M., and Kikuchi, H. (1998) *J. Biol. Chem.* **273,** 19853–19858
21. Lawrence, P., Leid, M., and Kerkvliet, N. I. (1996) *Toxicol. Appl. Pharmacol.* **138,** 275–284
22. McGuire, J., Okamoto, K., Whitelaw, M. L., Tanaka, H., and Poellinger, L. (2001) *J. Biol. Chem.* **276,** 41841–41849
23. Köhle, C., Hassepass, I., Bock-Hennig, B. S., Bock, K. W., Poellinger, L., and McGuire, J. (2002) *Arch. Biochem. Biophys.* **402,** 172–179
24. Levine, S. L., Petrulis, J. R., Dubil, A., and Perdew, G. H. (2000) *Mol. Pharmacol.* **58,** 1517–1524
25. Tanaka, J., Miwa, Y., Miyoshi, K., Ueno, A., and Inoue, H. (1999) *Biochem. Biophys. Res. Commun.* **264,** 938–943
26. Peter, M. E., and Krammer, P. H. (1998) *Curr. Opin. Immunol.* **10,** 545–551
27. Leppä, S., and Bohmann, D. (1999) *Oncogene* **18,** 6158–6162
28. Bennin, D. A., Don, A. S. A., Brake, T., McKenzie, J. L., Rosenbaum, H., Ortiz, L., DePaoli-Roach, A. A., and Horne, M. C. (2002) *J. Biol. Chem.* **277,** 27449–27467
29. Wang, X. W., Zhan, Q., Coursen, J. D., Khan, M. A., Konthy, H. U., Yu, L., Hollander, M. C., O'Connor, P. M., Fornace, A. J., Jr., and Harris, C. C. (1999) *Proc. Natl. Acad. Sci. U. S. A.* **96,** 3706–3711
30. Medema, R. H., Klompmaker, R., Smits, V. A., and Rijksen, G. (1998) *Oncogene* **16,** 431–441
31. Chai, Z., Sarcevic, B., Mawson, A., and Toh, B. H. (2001) *J. Biol. Chem.* **276,** 33665–33674
32. Demoulin, J. B., Van Snick, J., and Renauld, J. C. (2001) *Cell Growth Differ.* **12,** 169–174
33. Furukawa, T., Sunamura, M., Motoi, F., Matsuno, S., and Horii, A. (2003) *Am. J. Pathol.* **162,** 1807–1815
34. Hollander, M. C., Sheikn, M. S., Yu, K., Zhan, Q., Iglesias, M., Woodworth, C., and Fornace, A. J., Jr. (2001) *Int. J. Cancer* **96,** 22–31
35. Yagi, A., Hasegawa, Y., Xiao, H., Haneda, M., Kojima, E., Nishikimi, A., Hasegawa, T., Shimokata, K., and Isobe, K. (2003) *J. Cell. Biochem.* **90,** 1242–1249
36. Gorelik, L., and Flavell, R. A. (2002) *Nat. Rev. Immunol.* **2,** 46–53
37. Schorl, C., and Sedivy, J. M. (2003) *Mol. Biol. Cell* **14,** 823–835
38. Elferink, C. J., Ge, N.-L., and Levine, A. (2001) *Mol. Pharmacol.* **59,** 664–673
39. Dearstyne, E. A., and Kerkvliet, N. I. (2002) *Toxicology* **170,** 139–151
40. Zeytun, A., McKallip, R. J., Fisher, M., Camacho, I., Nagarkatti, M., and Nagarkatti, P. S. (2002) *Toxicology* **178,** 241–260
41. Vogelstein, B., Lane, D., and Levine, A. J. (2000) *Nature* **408,** 307–310
42. Liedtke, C., Gröger, N., Manns, M. P., and Trautwein, C. (2003) *J. Biol. Chem.* **278,** 27593–27604
43. Park, J.-Y. K., Shigenaga, M. K., and Ames, B. N. (1996) *Proc. Natl. Acad. Sci. U. S. A.* **93,** 2322–2327
44. Park, J. H., Hahn, E. J., Kong, J. H., Cho, H. J., Yoon, C. S., Cheong, S. W., Oh, G. S., and Youn, H. J. (2003) *Toxicol. Lett.* **145,** 55–68
45. Kerkvliet, N. I., Steppan, L. B., Shepherd, D. M., Oughton, J. A., Vorderstrasse, B. A., and DeKrey, G. K. (1996) *J. Immunol.* **157,** 2310–2319

BIOLOGY OF REPRODUCTION 70, 1790–1797 (2004)
Published online before print 11 February 2004.
DOI 10.1095/biolreprod.103.025387

Exposure of Mouse Preimplantation Embryos to 2,3,7,8-Tetrachlorodibenzo-*p*-dioxin (TCDD) Alters the Methylation Status of Imprinted Genes *H19* and *Igf2*[1]

Qing Wu,[3,4] Seiichiroh Ohsako,[3,4] Ryuta Ishimura,[3,4] Junko S. Suzuki,[3] and Chiharu Tohyama[2,3,4]

Environmental Health Sciences Division,[3] National Institute for Environmental Studies, Tsukuba 305-8506, Japan
CREST,[4] JST, Kawaguchi 332-0012, Japan

ABSTRACT

2,3,7,8-Tetrachlorodibenzo-*p*-dioxin (TCDD) is an extremely toxic, persistent environmental contaminant that disrupts normal development in laboratory animals. In our earlier study, we found that exposure of preimplantation embryos to TCDD markedly induced cytochrome P4501A1 mRNA at the blastocyst stage. In the present study, to determine whether exposure of preimplantation embryos to TCDD affects fetal growth, we exposed preimplantation embryos to TCDD from the 1-cell stage to the blastocyst stage and then transferred them to unexposed recipient mice. On Embryonic Day 14, the fetuses exposed to TCDD during the preimplantation stage weighed less than the fetuses in the unexposed control group. Real-time reverse transcription-polymerase chain reaction analysis revealed that exposure of preimplantation embryos to TCDD tended to decrease the expression levels of the imprinted genes *H19* and *Igf2* (insulin-like growth factor 2 gene). Use of bisulfite genomic sequencing demonstrated that the methylation level of the 430-base pair *H19/Igf2* imprint control region was higher in TCDD-exposed embryos and fetuses than in the controls, and methyltransferase activity was also higher in the TCDD-exposed embryos than in the controls. To our knowledge, the present study is the first to provide evidence that TCDD exposure at the preimplantation stage alters the genomic DNA methylation status of imprinted genes, influences the expression level of imprinted genes, and affects fetal development.

developmental biology, early development, embryo, growth factors, toxicology

INTRODUCTION

2,3,7,8-Tetrachlorodibenzo-*p*-dioxin (TCDD) is an environmental contaminant that has a wide spectrum of toxic effects, including inducing severe weight loss and exerting fetotoxicity and teratogenicity [1–5]. It has also been reported to affect fetal body weight when administered to the mother [2] and to have direct effects on preimplantation embryos in vitro [3, 4]. In our previous study [5], we exposed different-stage preimplantation embryos to TCDD in vitro and found that TCDD induced the expression of cytochrome P4501A1 (CYP1A1) mRNA, as a biomarker for dioxin exposure [6], during the blastocyst stage. This finding suggests that TCDD directly affects regulation of gene expression in preimplantation embryos [5]. Although no morphological changes in the embryos were detected by the end of culture, whether the TCDD-exposed embryos would have displayed an abnormal phenotype during later stages of development remains unknown.

One of the marked differences between preimplantation embryos and later stages of development is a genome-wide reprogramming of the DNA methylation pattern in vivo [7]. Typically, a substantial portion of the genome is demethylated and, later, remethylated in a cell- or tissue-specific manner. During this period, only certain genomic regions, so-called "imprinted genes," are protected from demethylation at the time of fertilization [8–10]. The genes that are imprinted are established during oogenesis and spermatogenesis [11]. In contrast to other genes, the methylated status of imprinted genes is maintained during embryogenesis, including the preimplantation stage [12], and transmission of these imprints is essential for normal embryonic development [11, 13]. In studies using preimplantation embryos cultured in vitro, several investigators have reported finding that aberrant growth and specific phenotypic abnormalities during fetal and postnatal development are sometimes associated with aberrant epigenetic modifications (i.e., with an altered methylation pattern in the genome during the preimplantation stage) [14, 15]. In addition, deregulation of imprints of several genes significantly affects postnatal growth and development [13, 16].

In the present study, we exposed murine preimplantation embryos to TCDD in vitro and then transferred them to unexposed recipient mice to determine how TCDD affects fetal development. Because imprinted genes are thought to be highly responsive to environmental conditions at the preimplantation stage and alteration of the methylation pattern has significant effects on fetal development [14, 15], we focused on alteration of the expression levels of two growth-related imprinted genes, *H19* and *Igf2*, and we examined their genomic methylation status in the *H19/Igf2* imprint control region after preimplantation exposure to TCDD.

MATERIALS AND METHODS

Materials

The TCDD (purity, >99.5%) was purchased from Cambridge Isotope Laboratory (Andover, MA). The eCG and hCG were obtained from Teikokuzoki Co. (Tokyo, Japan). The M16 medium was from Sigma (St. Louis, MO). TRIzol reagent, SuperScript II reverse transcriptase, and oligo(dT)$_{12-18}$ primer were from Life Technologies (Rockville, MD). Wizard DNA Clean-Up System and plasmid pGEM-T Easy vector were from Promega (Madison, WI). The QuantiTect SYBR Green PCR kit, HotStar Taq polymerase, and QIAprep Spin Miniprep Kit were from Qiagen (Valencia, CA). Poly(dI-dC:dI-dC), [^{3}H-methyl]*S*-adenosylmethionine, and DYEnamic ET terminator cycle sequencing kit were from Amersham Biosci-

[1]Supported in part by grants from CREST, JST (to C.T.), the Ministry of Health, Labor, and Welfare (to C.T.), and the Japan Society for the Promotion of Science (to C.T.).
[2]Correspondence: Chiharu Tohyama, National Institute for Environmental Studies, 16-2 Onogawa, Tsukuba 305-8506, Japan. FAX: 81 298 50 2588; e-mail: ctohyama@nies.go.jp

Received: 21 November 2003.
First decision: 17 December 2003.
Accepted: 3 February 2004.

ISSN: 0006-3363. http://www.biolreprod.org

ences (Piscataway, NJ). Other reagents were of analytical grade and were obtained from Nacalai Tesque, Inc. (Kyoto, Japan).

Embryo Collection, TCDD Exposure, and Transplantation

Animals were cared for humanely according to the guidelines for animal experiments of the National Institute for Environmental Studies. Male and female Jcl:ICR mice (age, 9–10 wk) were purchased from Charles River, Inc. (Tokyo, Japan). The animals were provided access to food and water ad libitum and kept on a 12L:12D photoperiod. Female mice were superovulated by i.p. injection with 5 IU of eCG, followed 48 h later by an i.p. injection of 5 IU of hCG. The superovulated females were allowed to mate with the males.

Embryos were collected from the oviduct at the 1-cell stage, approximately 21–23 h after hCG administration. The TCDD was dissolved in dimethyl sulfoxide and then added to M16 medium, and the dimethyl sulfoxide concentration in the medium was set at 0.1% in both the exposure and control groups. The TCDD was added to the medium to a concentration of 10 nM, because this concentration significantly induced CYP1A1 expression in blastocyst embryos without producing morphological changes [5]. The 1-cell embryos from the same donor mouse were equally divided into two groups. They were then cultured to the blastocyst stage in 200-μl drops of M16 medium drops (with or without 10 nM TCDD) and covered with mineral oil in a humidified atmosphere of 5% CO_2 and 95% air at 37°C. After incubation, blastocyst embryos with clearly visible blastocoele cavities that had developed from the 1-cell stage were washed. The TCDD-exposed blastocysts were transferred into the one uterus, and the corresponding controls were transferred into another uterus of the same recipient female ICR mice (n = 7 blastocysts per horn).

Real-Time Reverse Transcription-Polymerase Chain Reaction

Fetuses were dissected on Embryonic Day (E) 14, and total RNA was purified from each whole fetus with TRIzol reagent and reverse transcribed with Superscript II reverse transcriptase. Quantitative real-time polymerase chain reaction (PCR) analysis was performed using the Roche LightCycler (Roche, Mannheim, Germany) [17] and the QuantiTect SYBR Green PCR kit according to the supplier's protocol. The primer sets used in the present study were as follows: *H19*: forward, taccccgggatgacttcatc; reverse, tatctccgggactccaaacc (GenBank accession no. Af049091, 7690–7875); *Igf2*: forward, gtgtgtgtcagccaagcatg; reverse, caaatgtggggacacagagg (GenBank accession no. U71085, 27066–27319); *cyclophilin*: forward, tggagatgaatctgtaggacgag; reverse, taccacatccatgccctctagaa (GenBank accession no. M60456, 172–554); *G3PDH*: forward, cacagtcaaggccgagaatg; reverse, tctcgtggttcacacccatc (GenBank accession no. M33599, 214–436). The amplification program was as follows: one cycle of 95°C for 15 min, followed by 35 cycles of denaturation for 15 sec at 95°C, annealing of primers for 20 sec at 56°C, and extension for 20 sec at 72°C. After completion of the final cycle, a melting curve analysis was performed to monitor PCR product purity. The identity of the PCR products was verified by agarose gel electrophoresis. Five serial dilutions, ranging from 0.125- to 2-μl aliquots of the reverse transcription (RT) reaction products, were used to construct the standard curve. All samples for each target gene were quantitatively analyzed simultaneously. Expression of the targeted gene transcript was calculated by linear extrapolation and normalized to that of *G3PDH*. The expression ratios for the various genes are reported relative to the mean expression ratio (adjusted to one) in the control group.

Bisulfite Genomic Sequencing

Genomic DNA was isolated from blastocyst embryos and E14 fetuses. Bisulfite treatment was performed as described previously [10, 18]. Briefly, the DNA was digested overnight with a *Not*I restriction enzyme and then subjected to denaturation for 20 min at 37°C with NaOH at a final concentration of 0.3 M. Freshly prepared 10 mM hydroquinone and 3.6 M sodium bisulfite were added to final concentrations of 0.5 mM and 3.1 M, respectively. The reaction mixture was incubated at 55°C for 16 h, and the DNA was then purified with the Wizard DNA Clean-Up System. The purified sample was resuspended in 50 μl of TE (10 mM Tris-HCl, pH 8.0, containing 1 mM EDTA) and denatured in 0.3 M NaOH at 37°C for 20 min. After neutralization with 3.0 M ammonium acetate, the DNA was ethanol-precipitated and resuspended in 50 μl of TE. The 430-base pair imprint control region of the *H19/Igf2* gene (GenBank accession no. U19619, 1301–1732) (see Fig. 3) was amplified by PCR with HotStar Taq polymerase. Two rounds of PCR were performed with fully nested primer pairs. The primer set for the first-round PCR was as follows: forward, gagtatttaggaggtataagaat; reverse, atcaaaaactaacataaacc. The primer set for the second-round PCR (a nested PCR), was as follows: forward, tttgtaaggagattatgtttatttttggat; reverse, ccctaacctcataaaacccataactataaa. The PCR products were directly sequenced to analyze overall methylation status and subcloned into pGEM-T Easy vector to analyze the methylation pattern. The DNA sequencing was performed by Applied Biosystems (Foster City, CA) PRISM 310 Genetic Analyzer and the dideoxynucleotide chain termination method using the DYEnamic ET terminator cycle sequencing kit.

DNA Methyltransferase Activity Assay

Total DNA methyltransferase activity was assayed as previously described [15]. Briefly, embryos were transferred into 17 μl of assay buffer containing 130 μCi/ml of [^{3}H-methyl]*S*-adenosylmethionine and lysed by four freeze/thaw cycles with dry ice in methanol. The unmethylated, double-stranded oligonucleotides [poly(dI-dC:dI-dC)] were added to the lysate, and the solution was then incubated for 2 h at 37°C. The poly(dI-dC:dI-dC) was precipitated by 10% trichloroacetic acid, resuspended in NaOH, and mildly acidified with HCl. Liquid scintillation counting was then performed.

Statistical Analysis

StatView for Windows version 5.0 (SAS Institute, Cary, NC) was used for the statistical analysis. All results are shown as the mean ± SEM. Differences in fetal weight were analyzed by two-way ANOVA, differences in gene expression by Student *t*-test, and differences in methyltransferase activity by paired Student *t*-test. Statistical significance was set at $P < 0.05$.

RESULTS

Preimplantation and Postimplantation Development

To avoid the differences caused by donor mouse condition and culture time, embryos from the same donor mouse were equally divided into two groups and then cultured in medium with or without TCDD from the 1-cell stage through the blastocyst stage. The ratio of preimplantation embryos that developed was calculated by dividing the number of developed embryos by the number of 1-cell embryos initially present. No difference in ratio occurred between the control embryos and the TCDD-exposed embryos (data not shown). The data were collected from three experiments, with a total of 400–450 control and TCDD-exposed embryos.

At the end of in vitro culture, the blastocyst embryos cultured with or without TCDD that had morphology typical of E4 were washed. The TCDD-exposed blastocysts were transferred into the one uterus, and the control blastocysts were transferred into another uterus of the same normal recipient mice. The effects of TCDD were then evaluated based on fetal survival rate and fetal body weight. No significant difference in the survival rate of E14 fetuses was found between the TCDD (10 nM)-exposed embryos and the control embryos (data not shown). On E14, the weight of the fetuses exposed to TCDD from the 1-cell to the blastocyst stage was 18.9% lower than that of the controls (Fig. 1). The data were obtained from 15 control fetuses and 16 TCDD-exposed fetuses of four recipients. Two-way ANOVA (Table 1) revealed that the decrease in fetal weight had been induced by TCDD ($P < 0.01$), not by a litter effect ($P > 0.05$), and no interaction between TCDD effect and litter effect ($P > 0.05$) was found.

Gene Expression Level

The relative expression levels of *Igf2* and *H19* were determined in the whole fetal body on E14 by a real-time RT-PCR analysis of eight control fetuses and eight TCDD-ex-

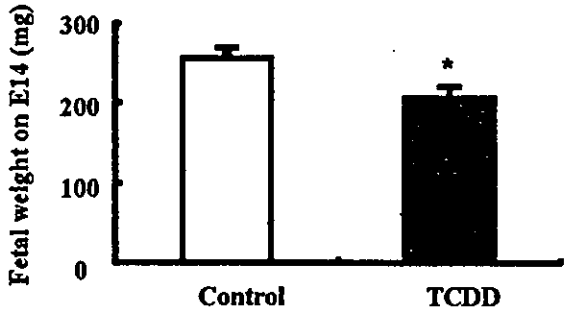

FIG. 1. Effect of TCDD on E14 fetal body weight. Data for TCDD-exposed and control fetuses (16 and 15 fetuses, respectively) from four recipients were compared. Results are expressed as the mean ± SEM. Asterisk indicates a statistically significant difference ($P < 0.05$) as a result of TCDD treatment according to two-way ANOVA.

posed fetuses (two control fetuses and two TCDD-exposed fetuses from each litter). The housekeeping genes *cyclophilin* and *G3PDH* were used as controls. Expression of the targeted genes was normalized to that of *G3PDH*. The melting curve of each targeted gene had only one peak, demonstrating the specificity of the amplification. The sample with no target template was used as a negative control, and no primer dimers were found in the negative control. The graphs of fluorescence versus cycles for each sample provided by the LightCycler data analysis front screen are shown in Figure 2A, and the expression levels of *H19, Igf2,* and *cyclophilin* relative to *G3PDH* are shown in Figure 2B. For *cyclophilin,* no difference of expression was found between the control and TCDD-exposed group. The expression level of *H19* was significantly decreased in the TCDD-exposed group. The expression level of *Igf2* tended to be reduced, but the difference was not statistically significant.

Methylation Status in the Imprint Control Region of the H19/Igf2 *Gene*

We used the bisulfite genomic sequencing method to determine whether the suppression of *H19* and *Igf2* expression in E14 fetuses was associated with alteration of the methylation level and pattern in the *H19/Igf2* imprint control region (Fig. 3) [9, 19, 20], which contains the CTCF-binding site involved in regulating the imprinted expression of *H19* and *Igf2*. The bisulfite reaction converts unmethylated cytosine residues into uracil in the single-strand DNA, but it leaves 5-methylcytosine unchanged. The analyzed portion of the *H19/Igf2* imprint control region is normally methylated at CpG sites on the paternal allele and unmethylated at CpG sites on the maternal allele (Fig. 4, top line) [21]. Figure 4B is a typical sequence chart showing no cytosine peaks (C-peaks) from maternally derived DNA after bisulfite treatment and subsequent PCR subcloning into plasmid vector. By contrast, the chart from paternally derived DNA (Fig. 4C) possesses C-peaks (arrowheads), representing methylated cytosine residues protected against bisulfite treatment, with unmethylated cytosines shown as thymine peaks (T-peaks, asterisks), in contrast to the chart from the direct sequence of the PCR product from untreated genomic DNA, in which the unmethylated cytosines are shown as C-peaks (Fig. 4A).

In a preliminary examination to evaluate a semiquantitative assay for cytosine/thymine content in the mixed DNA pool, maternally derived template plasmid clones (M) (Fig. 4B) and paternally derived template plasmid clones (P) (Fig. 4C) were mixed in different proportions (3:1, 1:1, and 1:3) and then amplified by the same PCR method as used in the bisulfite genomic amplification. The PCR products were then directly sequenced to yield the sequencing profiles shown in Fig. 4, D–F. Basically, two peaks, a T-peak and a C-peak, are detected at positions suspected of being 5-methylcytosine in the paternal genomic DNA. However, in the chart of the PCR product from the template with the M:P ratio of 3:1 (Fig. 4D), the T-peaks are clearly higher than the C-peaks. In the chart of the PCR product from the template with the M:P ratio of 1:1 (Fig. 4E), the T-peaks are as high as the C-peaks. In the chart of the PCR product from the template with the M:P ratio of 1:3 (Fig. 4F), the T-peaks are lower than the C-peaks. Three PCR reactions were carried out per sample, but the sequencing profiles of the PCR products were essentially identical. Although the ratio of the peak integration area in direct DNA sequencing profiles generally is not thought to be quantitative, these results demonstrated that at least in the *H19/Igf2* imprint control region tested in the present study, the different heights of C- and T-peaks reflected the different cytosine/thymine content in the mixed DNA pool before the PCR.

The experimental results of alteration of the methylation level by TCDD exposure are shown in Figure 5. Figure 5A (top) shows the direct sequencing profile of the PCR products from bisulfite-treated genomic DNA isolated from three sets of 240 control embryos and 240 TCDD-exposed embryos. In the control samples, the heights of the T- and C-peaks at positions suspected of being 5-methylcytosine in the paternal genomic DNA are almost the same level, whereas in the TCDD-exposed samples, the C-peaks are higher than the T-peaks. Three PCR reactions were carried out for each sample, but identical profiles were obtained. Based on the preliminary semiquantitative examination (Fig. 4), the present experimental results strongly suggested that the 5-methylcytosine content of the targeted region in the genomic DNA of TCDD-exposed embryos was higher than that in the control embryos.

To further investigate the alteration of the methylation pattern by exposure to TCDD, plasmid subclones were prepared from PCR products. In the control group, 15 (44.1%) of the 34 clones assayed from three PCR products exhibited methylation at any of the CpG sites, and 19 (55.9%) clones exhibited no methylation. In the TCDD-exposed group, on the other hand, 22 (64.7%) of 34 clones assayed from three PCR products had methylation at any of the CpG sites, and 12 (35.3%) of the clones exhibited no methylation (Fig. 5A, bottom). These findings strongly support the above-de-

TABLE 1. Two-way ANOVA table for the effect of TCDD and litter and their interactions on fetal body weight.

Source of variation	Degree of freedom	Mean square	*F*	*P*
TCDD effect	1	15 616	9.696	0.0049
Litter effect	3	1522	0.945	0.4351
TCDD effect × litter effect[a]	3	495	0.307	0.8198
Residual	23	1610		

[a] The interaction of TCDD effect and litter effect.

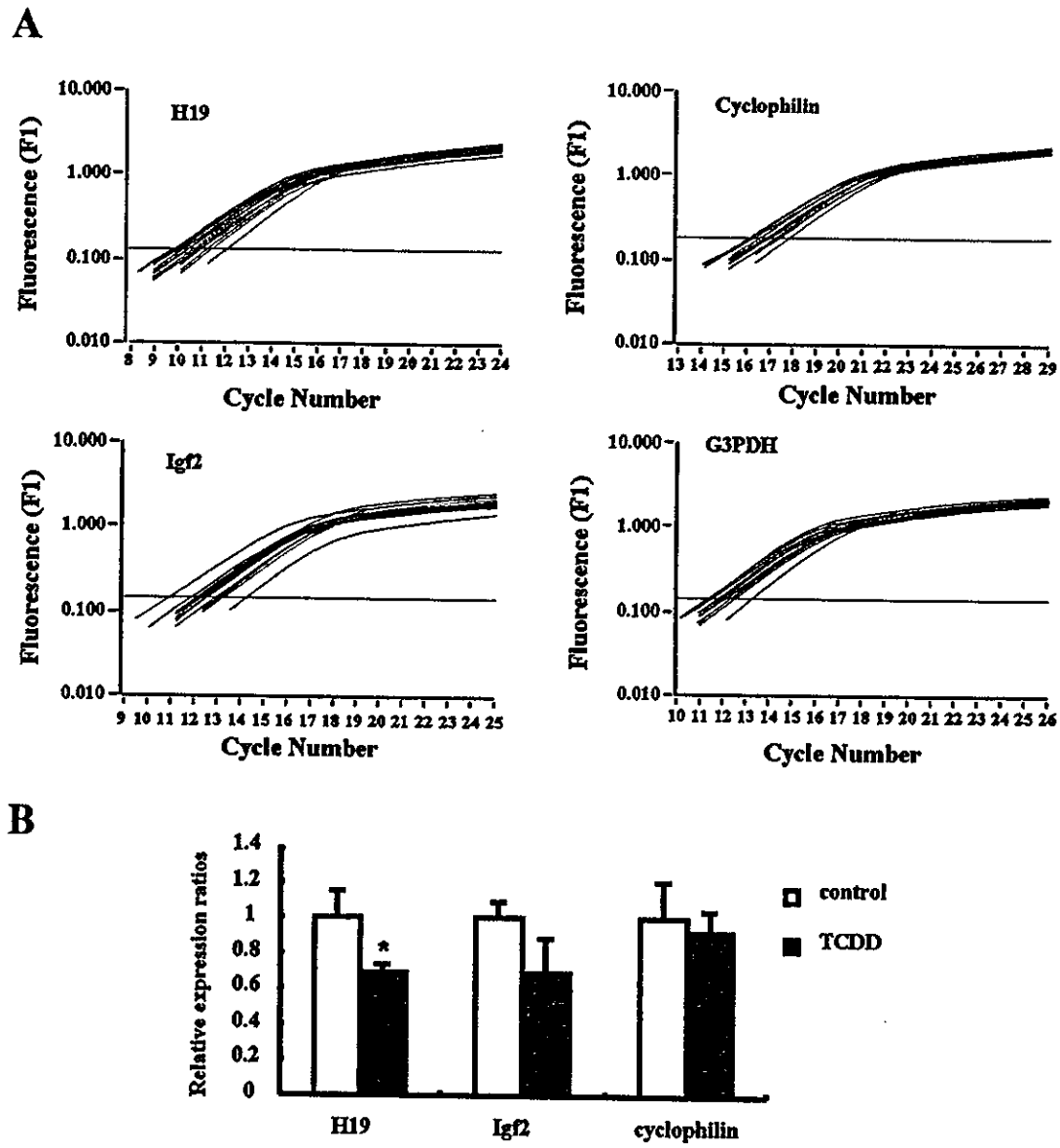

FIG. 2. Real-time PCR analysis of mRNA expression of *H19, Igf2, cyclophilin,* and *G3PDH* in E14 fetuses exposed to TCDD from the 1-cell to the blastocyst stage. A) Amplified curves monitored by LightCycler for each sample. The black and red lines represent control and TCDD-exposed samples, respectively. B) Expression ratios of targeted genes relative to the control. Data were calculated by linear extrapolation and normalized to *G3PDH* expression. Asterisk indicates a statistically significant difference ($P < 0.05$, n = 8) between the means in the TCDD group and control group according to Student *t*-test.

FIG. 3. Map of the 4-kilobase region upstream of the *H19* transcription start site. The restriction endonucleases sites are shown in top line include *Eco*RI (R), *Bam*HI (B), *Sac*I (S), and *Hha*I (H). The CpG dinucleotides are shown on the bottom line. The position and sequence of the 430-base pair region analyzed for methylation status in the present study are indicated by the rectangle (nucleotides 1301–1732).

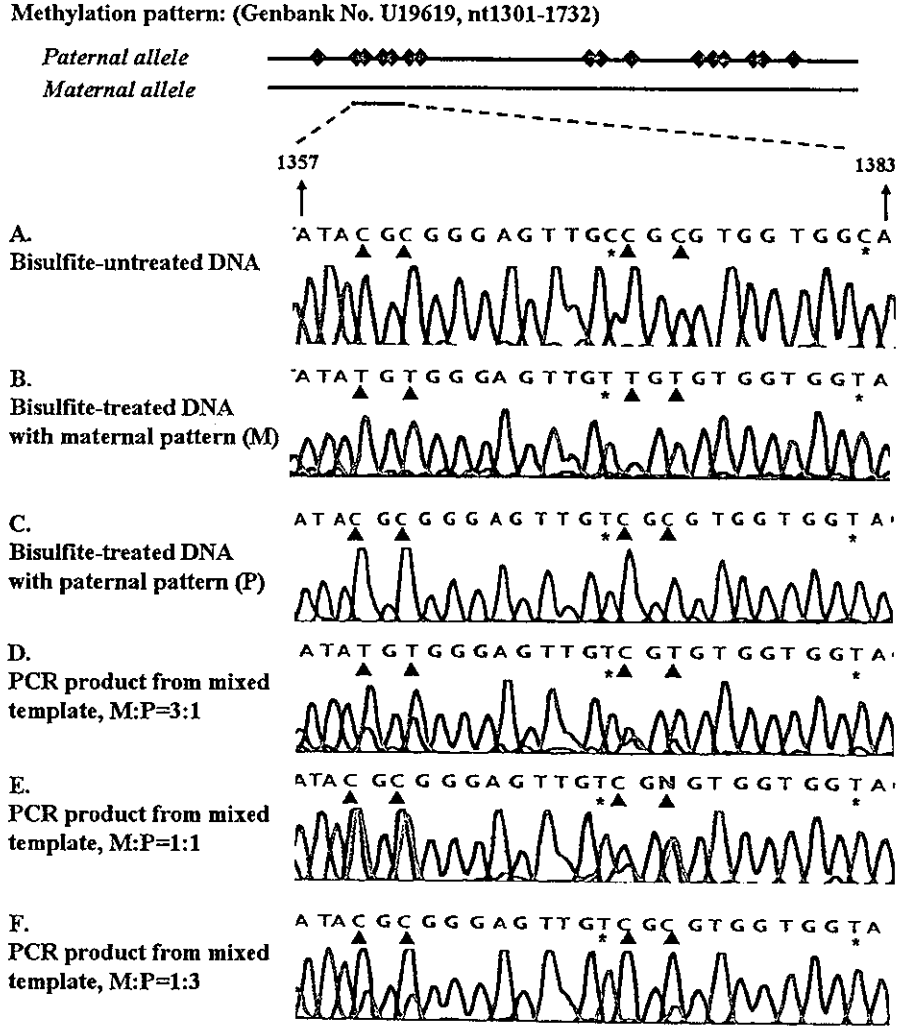

FIG. 4. Direct sequencing profile of PCR products obtained from bisulfite-treated DNA of defined methylation states and proportions. The methylation patterns of the paternal and maternal alleles of the *H19/Igf2* imprint control region are shown on the top line. Alleles are represented by horizontal lines, and the positions of methylated CpG dinucleotides are indicated by diamonds. The sequence profiles of nucleotides 1357–1368 are shown. Asterisks indicate unmethylated cytosine, and triangles indicate methylated cytosine. A) A sequence image of PCR product from bisulfite-untreated genomic DNA. B and C) Sequencing images of a bisulfite-treated, maternally derived DNA plasmid (M; B) and a paternally-derived DNA plasmid (P; C). Note that no C-peaks were found in B. D–F) Sequencing profiles of PCR products amplified from plasmid template mixtures having a M:P ratio of 3:1 (D), 1:1 (E), and 1:3 (F).

scribed direct sequencing profile, in that a higher methylation level of the *H19/Igf2* imprint control region was observed in TCDD-exposed samples.

We also determined the methylation status of the *H19/Igf2* imprint control region in E14 fetuses with preimplantation embryos that were exposed to TCDD and in controls. Figure 5B (top) shows the bisulfite genomic sequencing profiles of the TCDD-exposed fetuses and the control fetuses; they are similar to DNA sequencing profiles of the preimplantation embryos. In the control samples, the C-peak is the same as the T-peak, whereas in the TCDD-exposed samples, the C-peak is higher than the T-peak. After subcloning and sequencing the PCR products, we found that 20 (50%) of 40 clones assayed from four fetus samples in the fetal control group exhibited methylation, and 20 clones (50%) exhibited no methylation, at any of the CpG sites. On the other hand, in the TCDD-exposed group, 29 (60.4%) of 48 clones assayed from four fetus samples exhibited methylation, and 11 clones (22.9%) showed no methylation, at any of the CpG sites. Interestingly, the CpG dinucleotides at the 5′-end of the remaining eight clones (16.7%) were methylated, and the CpG dinucleotides at the 3′-end were unmethylated. The level of methylation of all CpG dinucleotides and of the CpG dinucleotides at the 5′-end in the TCDD-exposed group was 10.6% higher and 27.3% higher, respectively, than the corresponding methylation level in the control group (Fig. 5B, bottom).

Methyltransferase Activity in the TCDD-Exposed Embryos

To determine whether the higher methylation level in the *H19/Igf2* imprint control region after TCDD exposure was associated with methyltransferase activity, we measured the methyltransferase activity in preimplantation embryos. Because a marked, absolute decrease in enzyme activity has been reported from the 8-cell to the blastocyst stage [22], we equally divided embryos from each donor mouse into two groups and then cultured them in the medium with or without TCDD to prevent differences in fertilization time, embryo collection time, and culture time, which might have affected the results. At the end of in vitro culture, we selected embryos at a similar status of development (Fig. 6A) to measure the methyltransferase activity. Ten embryos in each group were used for the assays, each of which was conducted in triplicate. The experiments were repeated four times. The results of the paired Student *t*-test showed that TCDD-exposed embryos had significantly higher methyltransferase activity than the control embryos ($P < 0.05$) (Fig. 6B).

DISCUSSION

To our knowledge, this is the first study to provide evidence that TCDD can alter the genomic DNA methylation status of imprinted genes in preimplantation mouse embryos. During the in vitro culture experiment involving pre-

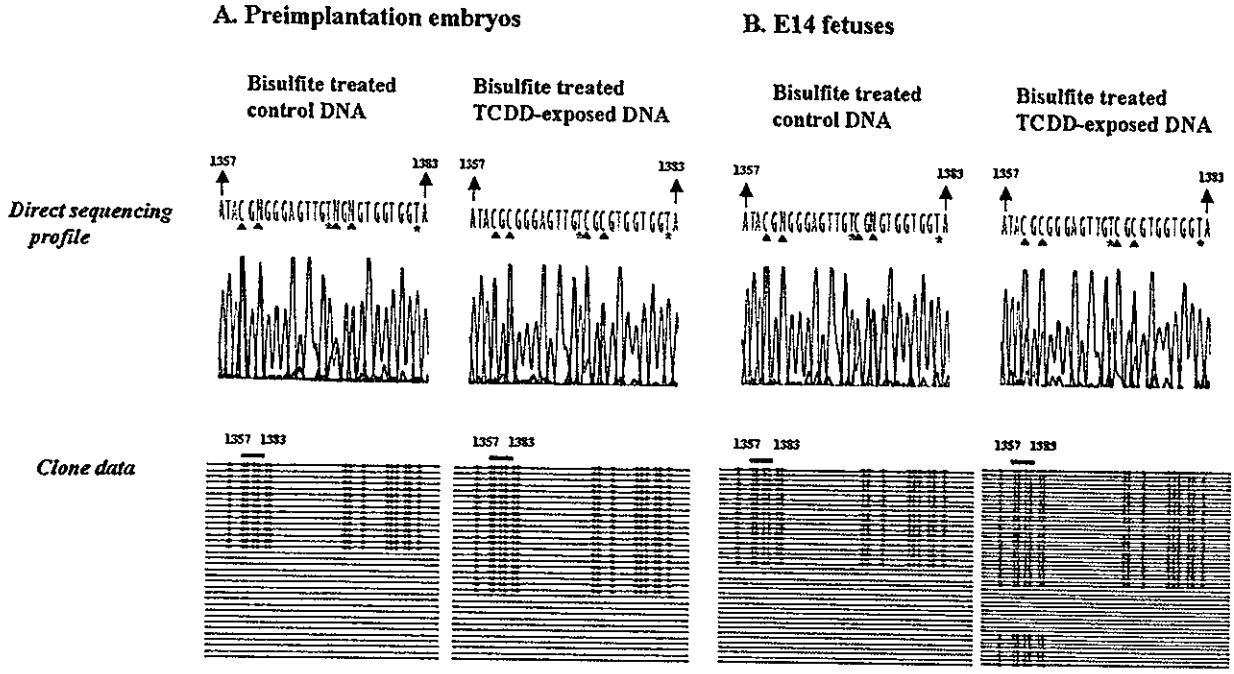

FIG. 5. Methylation status of the 430-base pair *H19/Igf2* imprint control region determined by bisulfite genomic sequencing. A) Methylation status in preimplantation embryos. B) Methylation status in E14 fetuses. Direct genomic sequencing profiles are shown (top). Note that all the unmethylated cytosine has been converted to thymine by bisulfite treatment (asterisks). The C-peaks in the imprinted loci of TCDD-exposed samples were higher than the T-peaks, whereas the heights of the C-peaks and the T-peaks were the same in the control samples (imprinted loci are indicated by triangles). The methylation patterns are also shown (bottom). Alleles are represented as horizontal lines, and the positions of methylated CpG dinucleotides are indicated by diamonds. The rectangle indicates the region of the direct sequence profile (top).

implantation embryos, embryos from each donor mouse were equally divided into two groups and cultured in medium with or without TCDD to minimize artifacts caused by fluctuations in donor mouse condition and embryo culture time. The thoroughness of bisulfite treatment in bisulfite genomic sequencing was first verified, and because direct sequencing confirmed that all the C-peaks in unimprinted loci were changed to T-peaks, the bisulfite treatments in the present study were concluded to have been complete. To test whether the difference in the height of the T- and C-peaks in the CpG nucleotide positions in the direct sequence chart reflected the content of DNA with different methylation patterns (paternal and maternal) before PCR, two different bisulfite-treated DNA templates (paternal and maternal) were mixed in a series of ratios, and PCR and direct sequencing were performed. The results showed that the sequencing profiles reflected the ratios of the two templates; that is, the more paternal pattern template added, the higher the C-peak obtained at the CpG site (Fig. 4). Employing this methodological principle, genomic DNA from each embryo sample was subjected to three PCR reactions, sequenced directly, and then subcloned and sequenced. Because the bisulfite direct sequence results coincided with the subcloning sequence results, we concluded that the methylation level of the *H19/Igf2* imprint control region was higher in the TCDD-exposed samples than in the control samples.

Explaining how TCDD affects the methylation status of imprinted genes during the preimplantation stage is not an easy task. However, we would address a possibility based on earlier studies concerning the mechanism of regulation of methylation and the regulation of TCDD effects [21, 23–30]. The alteration of DNA methylation status is related to methyltransferase [21, 23, 24]. Cytosine methyltransferase enzyme catalyzes the transfer of an activated methyl group from *S*-adenosylmethionine to the 5-position of the cytosine ring. Two distinct types of methyltransferases involved in maintenance and establishment of genomic methylation pattern in mammals, Dnmt1 and Dnmt3, have been func-

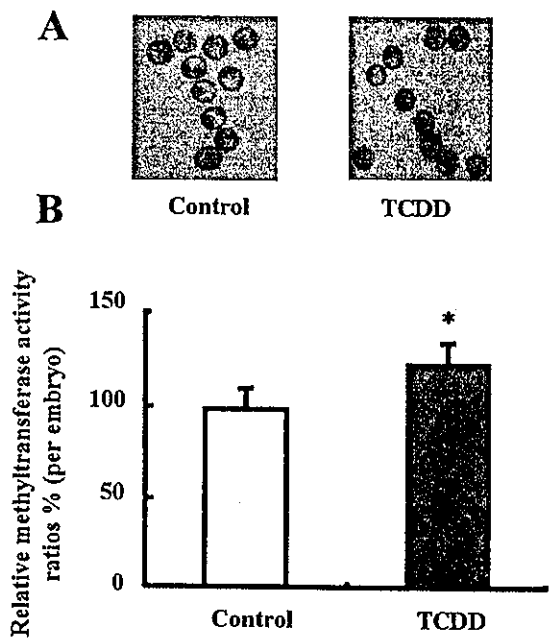

FIG. 6. Effect of TCDD on the methyltransferase activity of preimplantation embryos. A) Blastocyst embryos used for determination of methyltransferase activity. Note that the blastocyst embryos in the control samples and those in the TCDD-exposed samples are similar in size and morphology. Magnification ×60. B) Results are shown relative to the control value. Asterisks indicate a statistically significant difference ($P < 0.05$) as a result of TCDD treatment according to the paired Student *t*-test.

tionally characterized [23]. A variant of Dnmt1 protein, called Dnmt1o, is expressed in mouse oocytes and preimplantation embryos [21]. The Dnmt3b protein is specifically expressed in totipotential embryonic cells, such as inner cell mass, epiblast, and embryonic ectoderm cells, but it is downregulated in most adult somatic tissues [24]. It has been reported that expression of the *Dnmt1* gene in somatic cells is controlled by Sp1 [25, 26] and that the minimal promoter region of *Dnmt3b* contains an Sp1 site [27]. Taken together, these reports suggest that alteration of Sp1 activity may affect the level of expression of DNA methyltransferases. On the other hand, it has been well documented that the effects of TCDD are mediated by the arylhydrocarbon receptor (AhR) and AhR nuclear translocator (Arnt), both of which are constitutively expressed in preimplantation embryos [5]. The Sp1 protein is also expressed during preimplantation development [28], and an in vitro transcription study using CYP1A1 promoter showed synergistic enhancing effects between AhR/Arnt and Sp1 [29]. After gestational exposure to TCDD, the amount of Sp1 DNA binding in the cerebral cortex and cerebellum was revealed to be maximal on Postnatal Day 3, as opposed to Postnatal Day 10 in the controls, suggesting modulation of the DNA-binding activity of Sp1 as a result of the transplacental dioxin exposure [30]. Thus, based on the possible ability of Sp1 to regulate DNA methyltransferase gene expression mentioned above, TCDD may have affected the DNA methyltransferase activity through Sp1. The present study showed that methyltransferase activity in the preimplantation embryos exposed to TCDD was higher than that in control embryos, and this finding may support the possibility described above that TCDD may alter DNA methyltransferase gene expression through an increment in Sp1 activity. However, in the present study, we cannot clarify which methyltransferase gene was responsible for hypermethylation of the *H19/Igf2* imprinted control region by TCDD exposure. The mechanism of control for methylation needs further research.

To determine whether the later fetal development is affected by the exposure to TCDD during the preimplantation period in our experiments, TCDD-exposed preimplantation embryos were transferred to unexposed recipients. Because the embryo transplantation technique involves many complicated factors, such as the timing of blastocyst transfer and recipient condition, which may affect the results, TCDD-exposed blastocysts were transferred into the one uterus, and control blastocysts were transferred into another uterus of the same recipient mice. In addition, to avoid a possible effect of reduced numbers of fetuses, the comparisons were made only when at least three fetuses survived in each uterine horn. We found that under these experimental conditions, the methylation level of the *H19/Igf2* imprint control region was still higher in the E14 fetuses exposed to TCDD during the preimplantation stage and that the resulting fetal body weight was significantly lower than that in the control. The results suggested that the alterations of the methylation status of imprinted genes by TCDD during the preimplantation stage persist at later fetal stages. In the present study, we employed an in vitro culture system for TCDD exposure, because we could expect that the system would rule out the effect of the mother's physiological changes induced by TCDD and mimic the environment of the oviduct to find a direct effect of TCDD on preimplantation development. Although the dosage of TCDD used in the present study was 10 nM, which is much higher than the actual TCDD concentration in the milieu around the embryos [4], we propose that this experimental model may provide a novel finding regarding a direct effect of TCDD on epigenetics during development. It is worth examining whether an environmentally relevant dose of TCDD affects the methylation status of the imprinting genes.

The imprinted gene *Igf2* encodes a fetal growth factor and is expressed mostly on the paternal chromosome [31, 32], whereas the imprinted gene *H19* is expressed almost exclusively on the maternal allele [33, 34]. The *Igf2* gene is located before the *H19* gene on mouse chromosome 7, and regulatory regions called enhancers are farther along the chromosome, after both genes. Both the paternal silencing of *H19* and maternal repression of *Igf2* depend on an *H19/Igf2* imprint control region located 5′ of the *H19* gene. Transcription is triggered only when the enhancers interact with promoters located near each gene. The imprint control region on the maternal chromosome is unmethylated, which enables a zinc-finger protein, CTCF, to bind to several sites in the unmethylated imprint control region and block access of the enhancers to the *Igf2* promoter to silence the gene. However, the enhancers can still interact with the *H19* promoter; thus, *H19* is active. When the imprint control region at the CTCF-binding site is methylated, however, the enhancers cannot interact with the *H19* promoter and, instead, cause the *Igf2* genes to be turned on [19, 20, 35, 36]. In the present study, we found a higher methylation level in the *H19/Igf2* imprint control region of the TCDD-exposed group. This led us to expect decreased *H19* and increased *Igf2* expression levels, but the expression of *Igf2* tended to decrease on E14. The mechanisms underlying the decreased expression of *Igf2* are unknown, but histone acetylation is speculated to play a pivotal role. Recently, higher acetylation of the core histone H4 on active promoter regions, paternal *Igf2*, and maternal *H19* was observed compared with the silent alleles, suggesting differential histone acetylation of two parental alleles as a potential mechanism of transcription regulation [37, 38]. Moreover, in addition to the *H19/Igf2* imprint control region located 5′ of the *H19* gene, *Igf2* has several differentially methylated regions (*Igf2* DMR) located upstream and within the body of the gene that re-established the methylation pattern in the early postimplantation stages [39]. Deletion of the *H19/Igf2* imprint control region may lead to methylation of the *Igf2* DMR, and progressive methylation of the *Igf2* DMR appears to be correlated with downregulation of *Igf2* [40–42]. Thus, the distorted methylation level in the *H19/Igf2* imprint control region may result in aberrant *Igf2* gene expression at a later stage of development. Taken together, these results may explain why *Igf2* expression was decreased instead of increased in the present study. *Igf2* expression is thought to be associated with fetal growth [31, 43]. The tendency observed in the present study for fetal weight to decrease may be explained, in part, by alteration of the expression of *H19* or *Igf2*.

In summary, the present study is the first, to our knowledge, to demonstrate that an environmental toxicant, TCDD, alters the methylation status of imprinted genes in early development and that the altered methylation status is maintained throughout the fetal stage. Although the mechanisms regulating expression levels of the imprinted genes *H19* and *Igf2* and fetal growth in terms of their methylation status remain to be clarified, the alteration of methylation status by TCDD exposure during the preimplantation stage is thought to affect both the imprinted gene expression level and fetal growth. These results provide new

data for an epigenetic reprogramming mechanism and for the environmental health risk assessment.

ACKNOWLEDGMENT

The authors gratefully acknowledge the technical assistance of Takashige Kawakami with the real-time RT-PCR analysis.

REFERENCES

1. McConnell EE, Moore JA, Haseman JK, Harris MW. Comparative toxicity of chlorinated dibenzo-*p*-dioxins in mice and guinea pigs. Toxicol Appl Pharmacol 1978; 44:335–356.
2. Couture LA, Abbott BD, Birnbaum LS. A critical review of the developmental toxicity and teratogenicity of 2,3,7,8-tetrachlorodibenzo-*p*-dioxin: recent advances toward understanding the mechanism. Teratology 1990; 42:619–627.
3. Blankenship AL, Suffia MC, Matsumura F, Walsh KJ, Wiley LM. 2,3,7,8-Tetrachlorodibenzo-*p*-dioxin (TCDD) accelerates differentiation of murine preimplantation embryos in vitro. Reprod Toxicol 1993; 7:255–261.
4. Tsutsumi O, Uechi H, Sone H, Yonemoto J, Takai Y, Momoeda M, Tohyama C, Hashimoto S, Morita M, Taketani Y. Presence of dioxins in human follicular fluid: their possible stage-specific action on the development of preimplantation mouse embryos. Biochem Biophys Res Commun 1998; 250:498–501.
5. Wu Q, Ohsako S, Baba T, Miyamoto K, Tohyma C. Effects of 2,3,7,8-tetrachlorodibenzo-*p*-dioxin (TCDD) on preimplantation mouse embryos. Toxicology 2002; 174:119–129.
6. Nebert DW, Roe AL, Dieter MZ, Solis WA, Yang Y, Dalton TP. Role of the aromatic hydrocarbon receptor and [Ah] gene battery in the oxidative stress response, cell cycle control, and apoptosis. Biochem Pharmacol 2000; 59:65–85.
7. Reik W, Dean W, Walter J. Epigenetic reprogramming in mammalian development. Science 2001; 293:1089–1093.
8. Olek A, Walter J. The preimplantation ontogeny of the H19 methylation imprint. Nat Genet 1997; 17:275–276.
9. Tremblay KD, Duran KL, Bartolomei MS. A 5′–2-kilobase-pair region of the imprinted mouse H19 gene exhibits exclusive paternal methylation throughout development. Mol Cell Biol 1997; 17:4322–4329.
10. Warnecke PM, Mann JR, Frommer M, Clark SJ. Bisulfite sequencing in preimplantation embryos: DNA methylation profile of the upstream region of the mouse imprinted H19 gene. Genomics 1998; 51:182–90.
11. Bartolomei MS, Tilghman SM. Genomic imprinting in mammals. Annu Rev Genet 1997; 31:493–525.
12. Sanford JP, Clark HJ, Chapman VM, Rossant J. Differences in DNA methylation during oogenesis and spermatogenesis and their persistence during early embryogenesis in the mouse. Genes Dev 1987; 1: 1039–1046.
13. Constancia M, Pickard B, Kelsey G, Reik W. Imprinting mechanism. Genome Res 1998; 8:881–900.
14. Khosla S, Dean W, Brown D, Reik W, Feil R. Culture of preimplantation mouse embryos affects fetal development and the expression of imprinted genes. Biol Reprod 2001; 64:918–926.
15. Doherty AS, Mann MRW, Tremblay KD, Bartolomi MS, Schultz RM. Differential effects of culture on imprinted H19 expression in the preimplantation mouse embryo. Biol Reprod 2000; 62:1526–1535.
16. Moulton T, Crenshaw T, Hao Y, Moosikasuwan J, Lin N, Dembitzer F, Tensle T, Weiss L, McMorrow L, Loew T, Kraus W, Gerald W, Tycko B. Epigenetic lesions at the H19 locus in Wilms tumor patients. Nat Genet 1994; 7:440–447.
17. Wittwer CT, Ririe KM, Andrew RV, David DA, Gundry RA, Balis UJ. The LightCycler: a microvolume multisample fluorimeter with rapid temperature control. Biotechniques 1997; 22:176–181.
18. Clark SJ, Harrison J, Paul CL, Frommer M. High sensitivity mapping of methylated cytosines. Nuclei Acids Res 1994; 22:2990–2997.
19. Hark AT, Schoenherr CJ, Katz DJ, Ingram RS, Levorse JM, Tilghman SM. CTCF mediates methylation-sensitive enhancer-blocking activity at the *H19/Igf2* locus. Nature 2000; 405:486–489.
20. Bell AC, Felsendeld G. Methylation of a CTCF-dependent boundary controls imprinted expression of the IGF2 gene. Nature 2000; 405: 482–485.
21. Howell CY, Bestor TH, Ding F, Latham KE, Mertineit C, Trasler JM, Chaillet JR. Genomic imprinting disrupted by a maternal effect mutation in the *Dnmt1* gene. Cell 2001; 104:829–838.
22. Monk M, Adams RL, Rinaldi A. Decrease in DNA methylase activity during preimplantation development in the mouse. Development 1991; 112:189–192.
23. Bestor TH. The DNA methyltransferases of mammals. Hum Mol Genet 2000; 9:2395–2402.
24. Watanabe D, Suetake I, Tada T, Tajima S. Stage- and cell-specific expression of Dnmt3a and Dnmt3b during embryogenesis. Mech Dev 2002; 118:187–190.
25. Bigey P, Ramchandani S, Theberge J, Araujo FD, Szyf M. Transcriptional regulation of the human DNA methyltransferase (*dnmt1*) gene. Gene 2000; 242:407–418.
26. Kishikawa S, Murata T, Kimura H, Shiota K, Yokoyama KK. Regulation of transcription of the *Dnmt1* gene by Sp1 and Sp3 zinc-finger proteins. Eur J Biochem 2002; 269:2961–2970.
27. Ishida C, Ura K, Hirao A, Sasaki H, Toyoda A, Sakaki Y, Niwa H, Li E, Kaneda Y. Genomic organization and promoter analysis of the *Dnmt3b* gene. Gene 2003; 310:151–159.
28. Worrad DM, Schultz RM. Regulation of gene expression in the preimplantation mouse embryo: temporal and spatial patterns of expression of the transcription factor Sp1. Mol Reprod Dev 1997; 46:268–277.
29. Kobayashi A, Sogawa K, Fujii-Kuriyama Y. Cooperative interaction between AhR/Arnt and Sp1 for the drug-inducible expression of *CYP1A1* gene. J Biol Chem 1996; 271:12310–12316.
30. Nayyar T, Zawia NH, Hood DB. Transplacental effects of 2,3,7,8-tetrachlorodibenzo-*p*-dioxin on the temporal modulation of Sp1 DNA binding in the developing cerebral cortex and cerebellum. Exp Toxicol Pathol 2002; 53:461–468.
31. Constancia M, Hemberger M, Hughes J, Deas W, Ferguson-Smith A, Fundele R, Stewart F, Kelsey G, Fowden A, Sibley C, Reik W. Placental-specific IGF II is a major modulator of placental and fetal growth. Nature 2002; 417:945–948.
32. DeChiara TM, Efstratiadis A, Robertson EJ. A growth deficiency phenotype in heterozygous mice carrying an insulin-like growth factor II gene disrupted by targeting. Nature 1990; 345:78–80.
33. Pachnis V, Brannan CI, Tilghman SM. The structure and expression of a novel gene activated in early mouse embryogenesis. EMBO J 1988; 7:673–681.
34. Poirier F, Chan CT, Timmons PM, Robertson EJ, Evans MJ, Rigby PW. The murine H19 gene is activated during embryonic stem cell differentiation in vitro and at the time of implantation in the developing embryo. Development 1991; 113:1105–1114.
35. Bartolomei MS, Webber AL, Brunkow ME, Tilghman SM. Epigenetic mechanisms underlying the imprinting of the mouse H19 gene. Genes Dev 1993; 7:1663–1673.
36. Ferguson-Smith AC, Sasaki H, Cattanach BM, Surani MA. Parental-origin-specific epigenetic modifications of the mouse H19 gene. Nature 1993; 362:751–755.
37. Grandjean V, O'Neill L, Sado T, Turner B, Ferguson-Smith A. Relationship between DNA methylation, histone H4 acetylation, and gene expression in the mouse imprinted Igf2-H19 domain. FEBS Lett 2001; 488:165–169.
38. Hu JF, Hoffman AR. Examining histone acetylation at specific genomic regions. Methods Mol Biol 2001; 181:285–296.
39. Feil R, Walter J, Allen ND, Reik W. Developmental control of allelic methylation in the imprinted mouse *Igf2* and *H19* genes. Development 1994; 120:2933–2943.
40. Weber M, Milligan L, Delalbre A, Antoine E, Brunel C, Cathala G, Forne T. Extensive tissue-specific variation of allelic methylation in the *Igf2* gene during mouse fetal development: relation to expression and imprinting. Mech Dev 2001; 101:133–141.
41. Lopes S, Lewis A, Hajkova P, Dean W, Oswald J, Forne T, Murrell A, Constancia M, Bartolomei M, Walter J, Reik W. Epigenetic modification in an imprinting cluster are controlled by a hierarchy of DMRs suggesting long-range chromatin interactions. Hum Mol Genet 2003; 12:295–305.
42. Forne T, Oswald J, Dean W, Saan JR, Bailleul B, Dandolo L, Tilghman M, Walter J, Reik W. Loss of the maternal H19 gene induces changes in Igf2 methylation in both *cis* and *trans*. Proc Natl Acad Sci U S A 1997; 94:10243–10248.
43. Burns JL, Hassan AB. Cell survival and proliferation are modified by insulin-like growth factor 2 between days 9 and 10 of mouse gestation. Development 2001; 128:3819–3830.